# Quantum Force in Wigner Space

Huaqing Li

Thesis for the degree of PhD of Philosophy in Natural Science. The thesis will be defended in English on the 28th of 2014 at 13:30 in KS101 of the chemistry building Chalmers, Göteborg

Supervisor: Professor Gunnar Nyman, University of Gothenburg
Examiner: Professor Shiwu Gao, University of Gothenburg
Opponent: Professor Dimitry Shalashilin, University of Leeds


UNIVERSITY OF GOTHENBURG

Contact information:
Huaqing Li
Department of Chemistry and Molecular Biology
University of Gothenburg
SE–412 96 Göteborg, Sweden
Phone: +46 (0)70-4304444
Email: lwwm192@gmail.com

Printed in Sweden by Ale Tryckteam, Bohus 2014

To my dear grand parents

# Abstract

In this thesis, I will present effective methods to study quantum dynamics using trajectories. Our methods are based on a method named the Classical Wigner model which starts with a quantum initial condition and generates trajectories which are propagated in time using a classical force. However, the Classical Wigner model can not describe the dynamical quantum effects, such as interference and dynamical tunneling, which are prominent in both gas-phase reactions and condensed matter systems. Another method under the name of 'Entangled trajectory molecular dynamics' (ETMD) describes the trajectories as dynamically entangled with each other and thus captures the essential quantum effects. However, the trajectories are no longer independent of each other and the expression of the force may encounter numerical problems for general applications. Thus it is challenging how one can improve the ETMD and CW to achieve independent trajectories with dynamical quantum effects, especially the tunneling effects. In this thesis, I am going to unveil two such approaches.

First, we find a new parameter which can be used to symbolize the dynamical quantum effects in the CW model. An effective force is constructed from this parameter to substitute for the classical force. The new method is named Classical Wigner model with an effective quantum force (CWEQF) and tunneling effects are captured. Then we also construct an effective force to present the entanglements in the ETMD method. The tunneling effects are explained for a quasi-bound potential. Then we implement the CWEQF on the collinear $H + H_2$ reaction to obtain the rate constant which achieves consistently improved results as compared to the ordinary CW model. We also carried out two-dimensional reaction probability applications compared with ETMD. Although there is still room left for us to improve these methods, our methods are able to contain quantum effects in molecular dynamics and to be applied to higher dimensional applications.

## List of Appended Papers

This thesis is a summary of the following four papers. References to the papers will be made using the Roman numbers associated with the papers.

I Jens Poulsen , Huaqing Li , Gunnar Nyman "*Classical Wigner method with an effective quantum force: Application to reaction rates*,"
J. Chem. Phys. 131, 024117 (2009)

II Huaqing Li , Jens Poulsen , Gunnar Nyman "*Application of the Classical Wigner Method With An Effective Quantum Force- Application to the collinear $H + H_2$ reaction*,"
J. Phys. Chem. 115, 7338 (2011)

III Huaqing Li , Jens Poulsen , Gunnar Nyman "*Tunneling Dynamics Using Classical-like Trajectories with an Effective Quantum Force*,"
J. Phys. Chem. Lett. 4, 3013 (2013)

IV Huaqing Li "*Phase space trajectories with an effective quantum force: Application to two dimensional models*,"
Manuscript

# Contents

# Chapter 1
# Introduction

## 1.1 Classical or Quantum?

If one is planning to simulate the dynamics of a system containing thousands of dynamically coupled degrees of freedom, classical dynamics will be the only option at present. Certain momenta and positions will be assigned to different atoms and trajectories from them will be governed by Newtonian forces. The advantage of classical dynamics is binary: first, classical dynamics is intuitive and straight-forward to visualize and think about, then it is also not demanding in terms of the numerical cost since the trajectories can be run independently of each other under the classical force. Due to the simplicity and numerical efficiency, classical molecular dynamics (MD) simulations play a leading role in complex molecular systems [1–3].

However, the limitations of classical MD can not be ignored. Neglecting quantum mechanical effects such as zero-point energy (ZPE) and tunneling effects, etc, may render a worse performance. For example, tunneling through the reaction barrier could enhance the rate of reaction at room temperature by several orders of magnitude (paper I). In such cases, quantum effects should definitely be treated. Quantum dynamics describes the evolution of the physical system in a way that is not only qualitatively but also quantitatively accurate [4, 5]. However, exact solutions of the time-dependent Schrödinger equation are in practice limited to only a few degrees of freedom [6, 7]. As Dirac pointed out: *The underlying physical laws necessary for the mathematical theory of a large part of physics and the whole of chemistry are thus completely known, and the difficulty is only that the application of these laws leads to equations much too complicated to be soluble* [8].

## 1.2 Semi-classical!

In view of the limitations and difficulties of classical and quantum mechanics respectively, the developments of methods that are based on classical trajectories but incorporate quantum effects is an important subject. Semiclassical methods is of particular interest in this respect [9, 10]. According to Thoss and Wang [11] : ' *...semiclassical theories in the time domain is to find an approximate description of the quantum propagator* $e^{iHt/\hbar}$ *in terms of classical trajectories, which is valid in the asymptotic limit* $\hbar \to 0$'. There are different semi-classical methods such as semi-classical initial value representation (SC-IVR) [12, 13]; forward-backward initial value representations (FB-IVR) [14]; centroid molecular dynamics (CMD) [15], ring polymer molecular dynamics (RPMD), [16], etc (we refer the readers to the references corresponding to these methods). All of these semi-classical methods are able to simulate multi-dimensional quantum systems. RPMD and CMD are easy to apply to large systems and have been applied

to realistic models of low temperature quantum liquids, while the SC-IVR has to date only been applied to multi-dimensional model systems. They all include some kind of quantum correction to the dynamics of the system. Maybe the most rigorous of them is the SC-IVR method which is the only one being able to account for interference effects (quantum mechanical superposition).

Sometimes, 'semi-classical' methods reduce to 'quasi-classical' methods where classical trajectories are run using quantum initial conditions. An example is the linearized semi-classical initial value representation (LSC-IVR) [17] which is also named the Classical Wigner (CW) model [18, 19]. The CW method, which we shall improve in this thesis, starts with quantum initial conditions given by a so-called Wigner function (section 2.3) and run trajectories independent of each other under a classical force (section 2.6). It therefore corresponds to a quasi-classical method. Applications of the CW to condensed phase problems are quite successful [18, 20–23]. However, the CW model utilizes independent trajectories and thus is not able to describe the dynamical tunneling effects[22].

Our methods presented here are both related to the improvements of the Classical Wigner model by a quantum correction to the classical force (a quantum force). Compared with the CW model, the quantum force is $\hbar$-dependent (including higher order contributions). Also the classical and quantum forces become identical in the classical limit ($\hbar \to 0$). Therefore, we refer to our methods as semi-classical.

In chapter 3, the quantum force is applied to the Wigner function of the thermal flux operator (section 2.2) to study its dynamics in a canonical system (NVT). Then (in chapter 4) the quantum force is constructed from the Wigner function of the density operator (section 2.2) in a micro-canonical system (NVE). For each of the systems (NVT and NVE), the quantum forces are generalized to higher dimensional applications. The tunneling effects are well described via the quantum force. Also the numerical cost is equivalent to the CW model in the canonical system. For the density operator in the micro-canonical system, the quantum force is updated in time to describe the long time tunneling effects.

# Chapter 2

# Theoretical Background

In this chapter, I will go through some important background knowledge to pave the way for our methods. I will start with the position (momentum) representation and the quantum operators that are involved in our calculations. Then I will introduce the Wigner function and the Feynman Path Integrals. At last, I will present the rate constant and how to use the Classical Wigner model to obtain it.

## 2.1 Position and Momentum Eigenstates

In quantum mechanics, the position and momentum of a particle are represented by the hermitian operators, $\hat{x}$, $\hat{p}$ respectively. A state vector $|\Psi>$ is the quantum representation of the particle, the wave function in different representations is the combination of the state vector with either the eigenstate of position $|x>$ or with the eigenstate of momentum $|p>$. The eigenstates (one dimensional motion is used for simplicity) of position and momentum are defined as:

$$\begin{aligned} \hat{x}|x> &= x|x> \\ \hat{p}|p> &= p|p> \end{aligned} \tag{2.1}$$

Since the operators are hermitian, the eigenvalues of x and p are real. Two position eigenstates obey the orthogonality property

$$< x'|x> = \delta(x' - x) \tag{2.2}$$

However, they are not normalized, the same property holds for the momentum eigenstates. The position and momentum states representations are not welcomed in Hilbert space since they are not square integrable functions. However, we can still use these states to form a complete set of states to expand an arbitrary quantum state $|\Psi>$ into position (or momentum) eigenstates. By using the completeness relation:

$$\int_{-\infty}^{\infty} dx|x>< x| = 1 \tag{2.3}$$

we obtain the representation of a state vector $|\Psi>$ in the position representation:

$$|\Psi> = \int_{-\infty}^{\infty} dx|x>< x|\Psi> = \int_{-\infty}^{\infty} dx\Psi(x)|x> \tag{2.4}$$

where we have used the definition of the wave function $\Psi(x) =< x|\Psi >$. We can also repeat the same procedure on the momentum representation to obtain:

$$|\Psi >= \int_{-\infty}^{\infty} dp\Psi(p)|p > \tag{2.5}$$

where $\Psi(p) =< p|\Psi >$. The transformation between the position and momentum wave functions is important for the following chapters. So I will briefly show the mechanism here: From eq. (2.5), we multiply with $< x|$ on both sides of it, then

$$\Psi(x) =< x|\Psi >= \int_{-\infty}^{\infty} dp\Psi(p) < x|p > \tag{2.6}$$

The scalar product of $< x|p >$ is the quantity I will consider. We have that

$$< x|\hat{p}|p >= -i\hbar\frac{d}{dx}p(x) \tag{2.7}$$

and

$$< x|\hat{p}|p >= p < x|p >= p \cdot p(x). \tag{2.8}$$

Now we equalize the rhs of eq. (2.7) and eq. (2.8),

$$p < x|p >= p \cdot p(x) = -i\hbar\frac{d}{dx}p(x) \tag{2.9}$$

From eq. (2.9), we have

$$\frac{dp(x)}{dx} = \frac{i}{\hbar}p \cdot p(x) \tag{2.10}$$

So the solution to $p(x)$ will be $p(x) =< x|p >= Ne^{ipx/\hbar}$. The normalization factor N can be derived from eq. (2.2) by inserting the completeness relation of the momentum states:

$$\begin{aligned}\delta(x - x') = \int_{-\infty}^{\infty} dp < x|p >< p|x' >= \int_{-\infty}^{\infty} dpp(x)p(x') \\ = |N|^2 \int_{-\infty}^{\infty} dpe^{-i(x-x')p/\hbar}.\end{aligned} \tag{2.11}$$

The definition of a delta function via the Fourier transform is

$$\delta(x - x') = \frac{1}{2\pi\hbar}\int_{-\infty}^{\infty} dpe^{i(x-x')p/\hbar} \tag{2.12}$$

So $N = \sqrt{\frac{1}{2\pi\hbar}}$. Then we have

$$< x|p >= \sqrt{\frac{1}{2\pi\hbar}}\exp\left(\frac{i}{\hbar}xp\right). \tag{2.13}$$

and the relation

$$\Psi(x) = \sqrt{\frac{1}{2\pi\hbar}}\int_{-\infty}^{\infty} dp\Psi(p)\exp\left(\frac{i}{\hbar}xp\right). \tag{2.14}$$

In this section, we briefly introduced the position and momentum representations, which are basic for Wigner function (section 2.3) and Feynman Path Integral (section 2.4).

## 2.2 Density operator and thermal flux operator

In the previous section, I have briefly introduced the state vector $|\Psi>$ which contains all the information about a quantum system. However, generally speaking it is not possible to describe the system by single state vectors because we may not know every detail of the system (the number of degrees of freedom may be too large) especially when the quantum system is coupled to a reservoir so that the motion of the constituents may be hard to follow. Thus another way to describe the quantum system is needed. From Born [24], the probability $W(x)dx$ to find the particle between $x$ and $x + dx$ can be interpreted via the wave function $\Psi(x)$. As a start, we can express the state vector as a superposition of different eigenstates ($|m>$) of different eigenenergies ($m$ specifies the different states):

$$|\Psi>=\sum_{m=0}^{\infty}\lambda_m|m> \tag{2.15}$$

$\lambda_m$ is a complex valued expansion coefficient. We then look for the probability of finding a particle at position $x$.

$$\Psi(x)=<x|\Psi>=\sum_{m=0}^{\infty}\lambda_m<x|m>=\sum_{m=0}^{\infty}\lambda_m u_m(x) \tag{2.16}$$

By using the Born interpretation, the probability of finding a particle at position $x$ is:

$$\begin{aligned} W(x)=|\Psi(x)|^2&=\sum_{m,n=0}^{\infty}\lambda_m^*\lambda_n u_m^* u_n \\ &=\sum_{m}^{\infty}|\lambda_m|^2|u_m(x)|^2+\sum_{m\neq n}^{\infty}\lambda_m^*\lambda_n u_m^*(x)u_n(x) \\ &=\sum_{m}^{\infty}P_m|u_m(x)|^2+\sum_{m\neq n}^{\infty}\lambda_m^*\lambda_n u_m^*(x)u_n(x) \end{aligned} \tag{2.17}$$

So the probability is not simply the sum of probabilities of each state but also the sum of the cross terms between different energy states. Thus it may be handy to write the probability as

$$W(x)=|\Psi(x)|^2=|<x|\Psi>|^2=<x|\Psi><\Psi|x>=<x|\hat{\rho}|x>, \tag{2.18}$$

where we define the density operator $\rho=|\Psi><\Psi|$. The density operator thus contains all the information of the quantum system. I will use this operator and its related Wigner function in the micro-canonical application.

The density operator presents the probability of the quantum system. In chemical reactions, the density of the particle is utilized to present the reaction probability. However, one may use another operator to present how fast does the reaction happen, thus the flux operator is adopted under such consideration. For canonical systems, the operator we use in this thesis is the thermal flux operator

$$\hat{F}(\beta)=\exp(-\frac{\beta}{2}\hat{H})\hat{F}\exp(-\frac{\beta}{2}\hat{H}), \tag{2.19}$$

where

$$\hat{F}=\frac{i}{\hbar}[\hat{H},\hat{h}] \tag{2.20}$$

and $\hat{h}$ is the heaviside operator and $\hat{H}$ presents the Hamiltonian of the system. In position representation, the flux operator can be written as

$$\hat{F}(s) = -\frac{i\hbar}{2m}\left[\delta(x-s)\frac{d}{dx} + \frac{d}{dx}\delta(x-s)\right]. \tag{2.21}$$

Here s denotes the position where the flux is specified. For an arbitrary wave function $\Psi(x,t)$, the flux through position s is

$$j(s,t) =< \Psi|\hat{F}(s)|\Psi > \tag{2.22}$$

thus

$$j(s,t) = -\frac{i\hbar}{2m}\left[\Psi(s,t)^*\frac{\partial\Psi(s,t)}{\partial s} - \frac{\partial\Psi(s,t)^*}{\partial s}\Psi(s,t)\right]. \tag{2.23}$$

## 2.3 The Wigner function

In classical mechanics, the state of a particle is described by its position and momentum. However, in quantum mechanics, the particle state is substituted by wave functions, thus can not be interpreted locally [24]. Generally speaking, there is no local representation to describe a particle in quantum mechanics, the wave function has a spread in both the position and momentum coordinates.

The Wigner function [25] serves as a bridge between quantum (wave-functions) and classical (local in position and momentum) mechanics. It relates operators to a distribution function in phase space (position and momentum space). For an arbitrary operator $\hat{A}$, the Wigner function is expressed as

$$A^W(x,p) = \int_{-\infty}^{\infty} < x-\eta/2|\hat{A}|x+\eta/2 > e^{ip\eta/\hbar}d\eta. \tag{2.24}$$

Take the density operator for example, $\hat{A} = \hat{\rho} = |\Psi >< \Psi|$, the Wigner function of $\hat{\rho}$ can be treated as a quasi-probability function. It is not an ordinary probability because the Wigner function can be negative. The negative value of the Wigner function reflects the non-classical property of the system.

The Wigner function $W(x,p) = \rho^W(x,p)$ of the density operator has certain properties:
(1) It is real in phase space. This follows since the density operator is Hermitian.
(2) The $x$ and $p$ probability distributions are given by

$$\begin{aligned} P(x) &= \frac{1}{2\pi\hbar}\int dpW(x,p), \\ P(p) &= \frac{1}{2\pi\hbar}\int dxW(x,p). \end{aligned} \tag{2.25}$$

(3) For an operator $\hat{\Omega}$, the average value can be calculated as:

$$\overline{\Omega} = \frac{1}{2\pi\hbar}\int\int dxdpW(x,p)\Omega^W(x,p). \tag{2.26}$$

Take the free translation of the ground state wave function of the harmonic oscillator (with frequency $\omega$ and mass $m$) for example [26],

$$\Psi(x) = (\frac{m\omega}{\pi\hbar})^{\frac{1}{4}}\exp(ip_0x)\exp(-\frac{m\omega}{2\hbar}(x-x_0)^2) \tag{2.27}$$

where the $x_0$ and $p_0$ correspond to the initial center of position and momentum. The initial Wigner function is thus

$$\rho^W(x,p,0) = \frac{1}{\pi\hbar}\exp\left(-\frac{(x-x_0)^2}{2\sigma_x^2} - \frac{(p-p_0)^2}{2\sigma_p^2}\right), \tag{2.28}$$

where $\sigma_x = \sqrt{\hbar/(2m\omega)}$ and $\sigma_p = \sqrt{\hbar m\omega/2}$ specify the widths of the distribution along $x$ and $p$. The widths of a Gaussian obey the minimum uncertainty principle: $\sigma_x\sigma_p = 0.5\hbar$ [24]. The matrix elements of the density operator are also derived from eq. (2.27)

$$\begin{aligned} &< x|\hat{\rho}|x' >=< x|\Psi >< \Psi|x' >= \Psi^*(x)\Psi(x') \\ &= (\frac{m\omega}{\pi\hbar})^{\frac{1}{2}}\exp(ip_0(x'-x))\exp[-\frac{m\omega}{2\hbar}((x-q_0)^2 + (x'-q_0)^2)]. \end{aligned} \tag{2.29}$$

By transforming to the mean and difference coordinates, $q = 0.5(x+x')$, $\eta = x'-x$, eq. (2.29) becomes

$$\begin{aligned} < x|\hat{\rho}|x' >&== (\frac{m\omega}{\pi\hbar})^{\frac{1}{2}}\exp(ip_0\eta)\exp[\frac{(q-q_0)^2}{2\frac{\hbar}{2m\omega}} + \frac{\eta^2}{2\frac{2\hbar}{m\omega}}] \\ &= (\frac{m\omega}{\pi\hbar})^{\frac{1}{2}}\exp(ip_0\eta)\exp[\frac{(q-q_0)^2}{2\sigma_q^2} + \frac{\eta^2}{2\sigma_\eta^2}]. \end{aligned} \tag{2.30}$$

The width of the Gaussian along the $\eta$ coordinate (off-diagonal coordinate of the density matrix) is denoted as $\sigma_\eta = \sqrt{\frac{2\hbar}{m\omega}}$. The relation between $\sigma_\eta$, $\sigma_q$ and the width $\sigma_x$ from the Wigner function of the Gaussian wave function is then: $\sigma_\eta = 2\sigma_q = 2\sigma_x$. We will refer to this relation in chapter 4.

## 2.4 Feynman Path Integral

Quantum dynamics carries the task to obtain the wave function (distribution function) for different times. In physics, such kind of problems will be solved via tools such as the Green Function. Propagators are such kind of Green Function which relates the wave function between different positions and times. Feynman replaces the classical notion of a single, unique trajectory with a sum of all possible trajectories to compute the quantum propagator [27]. The Feynman Path Integral (FPI) is parallel to Schrödinger and Heisenberg's representations [24] and it brings the 'path' and 'action' from the classical picture to the quantum mechanics.

To illustrate how FPI works, I start with the the Schrödinger equation for a time independent Hamiltonian $\hat{H}$

$$i\hbar\frac{\partial}{\partial t}|\Psi(t)>= \hat{H}|\Psi(t)> . \tag{2.31}$$

One gets the quantum state at time $t'$ as

$$|\Psi(t')>= \exp\left[-i\hat{H}(t'-t)/\hbar\right]|\Psi(t)> . \tag{2.32}$$

Utilizing the coordinate representation plus the identity $I = \int dx|x >< x|$, one has

$$\begin{aligned} &< x'|\Psi(t')>=< x'|\exp\left[-i\hat{H}(t'-t)/\hbar\right]|\Psi(t)> \\ &= \int dx < x'|\exp\left[-i\hat{H}(t'-t)/\hbar\right]|x >< x|\Psi(t)> . \end{aligned} \tag{2.33}$$

Eq. (2.33) can be rewritten as

$$\Psi(x',t') = \int dx K(x',t',x,t)\Psi(x,t), \tag{2.34}$$

where we used [27]

$$K(x',t',x,t) =< x'| \exp\left[-i\hat{H}(t'-t)/\hbar\right] |x> . \tag{2.35}$$

$K$ is named a propagator, which relates the wave function between different times and positions. The FPI divides the propagation time $(t'-t)$ into a series of slices $\Delta t = \frac{t'-t}{N}$, $N \to \infty$. For a short time interval $\Delta t \to 0$, from [28] the one-dimensional propagator is expressed as

$$\begin{aligned} K(x_2, t+\Delta t, x_1, t) &=< x_2| \exp(-\frac{i\Delta t}{2m\hbar}\hat{p}^2) \exp[-\frac{i\Delta t}{\hbar}V(x)]|x_1> \\ &\approx (\frac{m}{2\pi\hbar i\Delta t})^{1/2} \exp\left[\frac{im(x_2-x_1)^2}{2\hbar\Delta t} - \frac{i\Delta t}{2\hbar}(V(x_2)+V(x_1))\right]. \end{aligned} \tag{2.36}$$

For $j = 1, N-1$, the identity I is

$$I = \int_{-\infty}^{\infty} dx_j |x_j >< x_j|. \tag{2.37}$$

We insert this identity expression into eq. (2.35) and use the short-time propagator from eq. (2.36),

$$\begin{aligned} K(x',t',x,t) = \prod_{j=1}^{N-1} \int_{-\infty}^{\infty} dx_j &< x' = x_N| \exp\left[-i\hat{H}\Delta t/\hbar\right] |x_{N-1}> \\ &< x_{N-1}| \exp\left[-i\hat{H}(\Delta t)/\hbar\right] |x_{N-2}> ... \\ < x_2| \exp\left[-i\hat{H}(\Delta t)/\hbar\right] |x_1 >< x_1| &\exp\left[-i\hat{H}(\Delta t)/\hbar\right] |x_0 = x> \\ = \prod_{j=1}^{N-1} \int_{-\infty}^{\infty} dx_j &< x' = x_N| \exp(-\frac{i\Delta t}{2m\hbar}\hat{p}^2) \exp[-\frac{i\Delta t}{\hbar}\hat{V}]|x_{N-1}> \\ &< x_{N-1}| \exp(-\frac{i\Delta t}{2m\hbar}\hat{p}^2) \exp[-\frac{i\Delta t}{\hbar}\hat{V}]|x_{N-2}> ... \\ &< x_2| \exp(-\frac{i\Delta t}{2m\hbar}\hat{p}^2) \exp[-\frac{i\Delta t}{\hbar}\hat{V}]|x_1> \\ &< x_1| \exp(-\frac{i\Delta t}{2m\hbar}\hat{p}^2) \exp[-\frac{i\Delta t}{\hbar}\hat{V}]|x_0 = x> . \end{aligned} \tag{2.38}$$

Each short time propagator can be expressed by eq. (2.36). We have:

$$\begin{aligned} K(x',t',x,t) = (\frac{m}{2\pi\hbar i\Delta t})^{1/2} [\prod_{j=1}^{N-1} (\frac{m}{2\pi\hbar i\Delta t})^{1/2} \int_{-\infty}^{\infty} dx_j] \\ \exp[\sum_{j=1}^{N} \frac{im(x_j-x_{j-1})^2}{2\hbar\Delta t} - \frac{i\Delta t}{\hbar}V(x_j)]. \end{aligned} \tag{2.39}$$

Since $\Delta t \approx 0$, $\frac{x_j - x_{j-1}}{\Delta t} \approx \dot{x}_j$, the Lagrangian $L(x_j, \dot{x}_j)$ is defined as $L(x_j,\dot{x}_j) = \frac{m(x_j-x_{j-1})^2}{2(\Delta t)^2} - V(x_j)$ one can rewrite eq. (2.39) as

$$K(x',t',x,t) = \int D[x(t)] \exp[\frac{i}{\hbar}\int_t^{t'} dt L(x,\dot{x})], \tag{2.40}$$

where

$$\int D[x(t)] = \lim_{N\to\infty} (\frac{m}{2\pi\hbar i\Delta t})^{1/2} [\prod_{j=1}^{N-1} (\frac{m}{2\pi\hbar i\Delta t})^{1/2} \int_{-\infty}^{\infty} dx_j]. \tag{2.41}$$

$K(x', t', x, t)$ is the Green function that connects position x at time t to position $x'$ at time $t'$. The propagator is the sum of the contributions of all possible paths. Each path carries its own phase along with it. The FPI can also be done in phase space (position-momentum space). Inserting the identity of $I = \int dp_j |p_j >< p_j|$, $j = 1, N$, where $N \to \infty$, one gets

$$K(x', t', x, t) = \int D[p(t)]D[x(t)] \exp[\frac{i}{\hbar} \int_t^{t'} dt[L(x, \dot{x}) - p\dot{x}]], \tag{2.42}$$

and

$$\int D[p(t)]D[x(t)] = \lim_{N\to\infty} (\frac{1}{2\pi\hbar})^N \int_{-\infty}^{\infty} .... \int_{-\infty}^{\infty} \prod_{j=1}^{N} \prod_{k=1}^{N-1} dp_j dx_k. \tag{2.43}$$

FPI will be used to solve the time propagators that reside in the correlation functions in the next sections.

## 2.5 The rate constant

In the previous section, I introduced the Feynman Path Integral to handle the time evolution operator, which will be contained in the expression of the thermal rate expression that is used in the following sections. The thermal rate constant in this thesis is expressed as [29]

$$k(T) = \frac{1}{Q_r} \int_0^{\infty} dt C_{ff}(t), \tag{2.44}$$

where $Q_r$ is the reactant partition function, $C_{ff}$ is the auto-correlation function

$$C_{ff}(t) = Tr\Big[\hat{F}(\beta/2) \exp(i\hat{H}t/\hbar)\hat{F}(\beta/2) \exp(-i\hat{H}t/\hbar)\Big], \tag{2.45}$$

with $\beta = 1/k_B T$. Compared to eq. (2.19), the half-Boltzmannized flux operator is

$$\hat{F}(\beta/2) = \exp(-\frac{\beta}{4}\hat{H})\hat{F} \exp(-\frac{\beta}{4}\hat{H}). \tag{2.46}$$

where the flux operator $\hat{F}$ is given by eq. (2.20)- eq. (2.21).

## 2.6 The Classical Wigner model

The rate constant was introduced in the previous section and I am going to calculate it in a semi-classical way.

For arbitrary operators $\hat{A}$ and $\hat{B}$,

$$\begin{aligned} Tr\{\hat{A}\exp(iHt/\hbar)\hat{B}\exp(-iHt/\hbar)\} = \\ \int dx_i dx_i' \int dx_f dx_f' < x_i|\hat{A}|x_i' > \\ < x_i'|e^{it\hat{H}/\hbar}|x_f' >< x_f'|\hat{B}|x_f >< x_f|e^{-it\hat{H}/\hbar}|x_i > . \end{aligned} \tag{2.47}$$

The trace in eq. (2.47) involves two time evolution operators thus two Feynman paths are generated (see fig. 2.1).

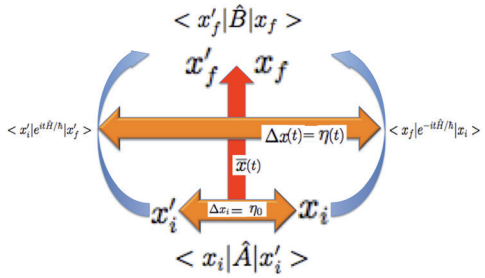


Figure 2.1: Two Feynman paths generated from eq. (2.47). The blue arrows specify the Feynman paths. The red arrow is the mean path and the orange double arrows stand for the distances between two Feynman paths.

The propagation along the Feynman paths can be divided into $N$ intermediate steps, for example

$$< x_f|e^{-it\hat{H}/\hbar}|x_i > \approx \prod_{m=1}^{N} \int\int \frac{dx_m dp_m}{2\pi\hbar} \int \frac{dp_{N+1}}{2\pi\hbar} e^{iS^N/\hbar}. \tag{2.48}$$

The action is expressed as

$$\begin{aligned} S^N = \sum_{n=1}^{N+1} \left[p_n(x_n - x_{n-1}) - \epsilon H(x_n, p_n)\right], \\ H = p_n^2/2M + V(x_n) \end{aligned} \tag{2.49}$$

where $x_0 = x_i$, $q_t = x_{N+1} = x_f$, $p_0 = p_i$, $p_t = p_f = p_{N+1}$, $N \to \infty$. $\epsilon = t/(N+1) \to 0$ is the time step for the propagator. Now we transform the coordinates as

$$\begin{aligned} \overline{x}_i &= (x_i + x_i')/2, \\ \eta_i &= \Delta x_i = x_i - x_i', \\ \overline{p}_i &= (p_i + p_i')/2, \\ \Delta p_i &= p_i - p_i'. \end{aligned} \tag{2.50}$$

Eq. (2.47) is then rewritten as

$$Tr\{\hat{A}\hat{B}(t)\} = \int d\overline{x}_0 d\Delta x_0 \prod_{m=1}^{N+1} \int \frac{d\overline{x}_m d\overline{p}_m}{2\pi\hbar} \prod_{n=1}^{N+1} \int \frac{d\Delta x_n d\Delta p_n}{2\pi\hbar}$$

$$\exp(-i\frac{\epsilon}{\hbar}[V(\overline{x}_n+\Delta x_n/2)-V(\overline{x}_n-\Delta x_n/2)])$$
$$\exp(i\frac{\overline{p}_n}{M}\Delta p_n+i\Delta p_n\frac{(\overline{x}_n-\overline{x}_{n-1})}{\hbar}+i\overline{p}_n\frac{(\Delta x_n-\Delta x_{n-1})}{\hbar})$$
$$\left\langle \overline{x}_0+\frac{\Delta x_0}{2}\left|\hat{A}\right|\overline{x}_0-\frac{\Delta x_0}{2}\right\rangle\left\langle \overline{x}_{N+1}+\frac{\Delta x_{N+1}}{2}\left|\hat{B}\right|\overline{x}_{N+1}-\frac{\Delta x_{N+1}}{2}\right\rangle. \tag{2.51}$$

Assuming that the $\Delta x$s are relatively small, one can linearize the potential difference as :

$$\begin{aligned} V(x_i)-V(x_i') &= V(\overline{x}_i+\Delta x_i/2)-V(\overline{x}_i-\Delta x_i/2) \\ &\approx V'(\overline{x}_i)*\Delta x_i. \end{aligned} \tag{2.52}$$

This linearization works when $\Delta x_i\approx 0$, so eq. (2.51) becomes

$$\begin{aligned} Tr\{\hat{A}\hat{B}(t)\} &= \int d\overline{x}_0 d\Delta x_0 \prod_{m=1}^{N+1}\int\frac{d\overline{x}_m d\overline{p}_m}{2\pi\hbar}\prod_{n=1}^{N+1}\int\frac{d\Delta x_n d\Delta p_n}{2\pi\hbar} \\ &\exp\left(-i\frac{\epsilon}{\hbar}V'(\overline{x}_n)\Delta x_n+i\frac{\overline{p}_n}{M}\Delta p_n+i\Delta p_n(\overline{x}_n-\overline{x}_{n-1})/\hbar+i\overline{p}_n(\Delta x_n-\Delta x_{n-1})/\hbar\right) \\ &\left\langle \overline{x}_0+\frac{\Delta x_0}{2}\left|\hat{A}\right|\overline{x}_0-\frac{\Delta x_0}{2}\right\rangle\left\langle \overline{x}_{N+1}+\frac{\Delta x_{N+1}}{2}\left|\hat{B}\right|\overline{x}_{N+1}-\frac{\Delta x_{N+1}}{2}\right\rangle. \end{aligned} \tag{2.53}$$

We take a further step

$$\sum_{i=1}^{N+1}\overline{p}_i(\Delta x_i-\Delta x_{i-1})=\overline{p}_{N+1}\Delta x_{N+1}-\overline{p}_1\Delta x_0+\sum_{i=1}^{N}\Delta x_i(\overline{p}_i-\overline{p}_{i+1}). \tag{2.54}$$

Eq. (2.53) can be written now as

$$\begin{aligned} Tr\{\hat{A}\hat{B}(t)\} &\approx \frac{1}{2\pi\hbar}\int d\overline{x}_0 d\Delta x_0 d\Delta x_{N+1}\exp\left(-i\frac{\epsilon}{\hbar}V'(\overline{x}_{N+1})\Delta x_{N+1}\right) \\ &\prod_{m=1}^{N+1}\int d\overline{x}_m d\overline{p}_m\left\langle \overline{x}_0+\frac{\Delta x_0}{2}\left|\hat{A}\right|\overline{x}_0-\frac{\Delta x_0}{2}\right\rangle\left\langle \overline{x}_{N+1}+\frac{\Delta x_{N+1}}{2}\left|\hat{B}\right|\overline{x}_{N+1}-\frac{\Delta x_{N+1}}{2}\right\rangle \\ &\exp(i(\overline{p}_{N+1}\Delta x_{N+1}-\overline{p}_1\Delta x_0)/\hbar)\prod_{n=1}^{N}\int\frac{d\Delta x_n}{2\pi\hbar}\exp\left(-i\frac{\epsilon}{\hbar}\Delta x_n(V'(\overline{x}_n)+\frac{\overline{p}_{n+1}-\overline{p}_n}{\epsilon})\right) \\ &\prod_{n=1}^{N+1}\int\frac{d\Delta p_n}{2\pi\hbar}\exp\left(-i\frac{\epsilon}{\hbar}\Delta p_n(\frac{\overline{p}_n}{M}-\frac{\overline{x}_n-\overline{x}_{n-1}}{\epsilon})\right). \end{aligned} \tag{2.55}$$

The integration of $\Delta p_n$ and $\Delta x_n$ will introduce a series of delta functions. Eq. (2.55) becomes

$$\begin{aligned} Tr\{\hat{A}\hat{B}(t)\} &\approx \frac{1}{2\pi\hbar}\int d\overline{x}_0 d\Delta x_0 d\Delta x_{N+1}\exp\left(-i\frac{\epsilon}{\hbar}V'(\overline{x}_{N+1})\Delta x_{N+1}\right) \\ &\prod_{m=1}^{N+1}\int d\overline{x}_m d\overline{p}_m\left\langle \overline{x}_0+\frac{\Delta x_0}{2}\left|\hat{A}\right|\overline{x}_0-\frac{\Delta x_0}{2}\right\rangle\left\langle \overline{x}_{N+1}+\frac{\Delta x_{N+1}}{2}\left|\hat{B}\right|\overline{x}_{N+1}-\frac{\Delta x_{N+1}}{2}\right\rangle \\ &\exp(i(\overline{p}_{N+1}\Delta x_{N+1}-\overline{p}_1\Delta x_0)/\hbar)\prod_{n=1}^{N}\delta(\epsilon V'(\overline{x}_n)+\overline{p}_{n+1}-\overline{p}_n)\prod_{n=1}^{N+1}\delta(\epsilon\frac{\overline{p}_n}{M}-\overline{x}_n+\overline{x}_{n-1}). \end{aligned} \tag{2.56}$$

The delta functions generate trajectories that propagate from initial phase space point $(\overline{x}_0, \overline{p}_0)$ to final phase space point $(\overline{x}_t, \overline{p}_t)$. The equations of motion for any $(\overline{x}_n, \overline{p}_n)$ are:

$$\begin{aligned} \epsilon V'(\overline{x}_n) &= \overline{p}_n - \overline{p}_{n+1} \\ l\epsilon\frac{\overline{p}_n}{M} &= \overline{x}_n - \overline{x}_{n-1}. \end{aligned} \tag{2.57}$$

which are just the ordinary classical equations of motion. So

$$Tr\{\hat{A}\exp(iHt/\hbar)\hat{B}\exp(-iHt/\hbar)\} \approx \frac{1}{2\pi\hbar}\int d\overline{p}\int d\overline{x}A_W(\overline{x},\overline{p})B_W(\overline{x}_t,\overline{p}_t). \tag{2.58}$$

The Wigner transformation for arbitrary operator $\hat{A}$ is defined in eq. (2.24). In eq. (2.58), the trajectory from an initial point $(\overline{x},\overline{p})$ to the final point $(\overline{x}_t,\overline{p}_t)$ is run under a classical force. Using the rate constant expression from eq. (2.44)- eq. (2.45) together with eq. (2.57) and eq. (2.58), one arrives at

$$\begin{aligned} k(T) \approx \frac{1}{2\pi\hbar Q_r(T)}\int_0^\infty dt\int d\overline{p}\int d\overline{x} \\ \times F_W((\beta/2);\overline{x}(t),\overline{p}(t))F_W((\beta/2);\overline{x}(0),\overline{p}(0)), \end{aligned} \tag{2.59}$$

where $F_W((\beta/2;x,p)$ is the Wigner function of the half-Bolzmannized flux operator $\hat{F}(\beta/2)$. Classical trajectories are run to generate the auto-correlation function of $F_W(\hat{\beta}/2;x,p)$.

The classical force originates from the linearizing of the potential difference in eq. (2.52) and is only valid when $\delta x_i \to 0$ ($\delta x_i$ is the distance between the pair of Feynman Paths in fig. 2.1 and is also noted as $\eta$). The CW model is accurate at high temperature, heavy mass or harmonic potential.

However, the value of $\eta$ determines the importance of dynamical quantum effects. Take the double-slit experiment for example (see fig. 2.2): A particle is propagated through two slits and hits a plate. One can measure the probability that the particle hits the plate at position x. The corresponding operator is $\hat{D}_x = |x><x|$. Its time-dependent value is given as

$$\begin{aligned} D_x(t) = Tr\{\hat{\rho}\exp(iHt/\hbar)\hat{D}_x\exp(-iHt/\hbar)\} = \\ \int dx_i dx_i'\int dx_f dx_f' < x_i|\hat{\rho}|x_i' > \\ < x_i'|e^{it\hat{H}/\hbar}|x_f' >< x_f'|\hat{D}_x|x_f >< x_f|e^{-it\hat{H}/\hbar}|x_i > . \end{aligned} \tag{2.60}$$

If the two paths stay close to each other and penetrate through the same slit, the detector $D(x)$ will observe a classical result (no interference). In this case, the CW model will work well. On the other hand, if the two paths are separated from each other and go through different slits, the detector will observe a quantum result (interference). So we can deduce that the value of $\eta$ relates to the quantum effects in the dynamics. Assuming it to be zero in the CW model will result in the quenching of dynamical quantum effects.

## 2.7 Effective potential

The CW model described in the previous section captures the quantum effects in the initial condition (e.g. as a Wigner transform of the thermal flux operator) however not in the dynamics.

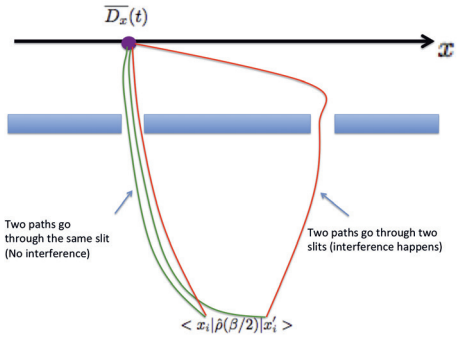


Figure 2.2: Two pairs of paths are generated to propagate through double slits. The green paths are close to each other and go through the same slit, thus the detecting function $D(x)$ obtains no quantum dynamical result (no interference will be detected). The red paths are separated from each other and penetrate through different slits. The detecting function $D(x)$ will capture the interference and a quantum dynamical result will be presented.

The classical force is local and can not describe tunneling and interference. It may be challenging to add quantum effects to the classical trajectories.

Considering the quantum influence to the dynamics, effective potentials may assist people to understand the quantum system. One of the most famous 'effective potential' is from Bohmian Mechanics [30, 31]. From the Schrödinger equation (SE)

$$i\hbar\frac{\partial}{\partial t}\Psi(r,t) = -\frac{\hbar^2}{2m}\nabla^2\Psi(r,t) + V(r)\Psi(r,t) \tag{2.61}$$

with the wave function $\Psi(r,t)$ for mass $m$ at position $r = (x_1, x_2, ..., x_n)$ and $\nabla^2$ is the Laplacian with $\nabla = (\frac{\partial}{\partial x_1}, \frac{\partial}{\partial x_2}, ..., \frac{\partial}{\partial x_n})$, Bohm [32] defined a general solution to the SE as $\Psi(r,t) = R(r,t)\exp(iS(r,t)t/\hbar)$. The amplitude R and action S are both treated as real. He then put this trial solution back into the SE and equalized the real and imaginary parts individually, which results in the following:

$$\begin{aligned}\frac{\partial R}{\partial t} &= -\frac{1}{2m}(R\nabla^2 S + 2\nabla R\cdot\nabla S)\\ \frac{\partial S}{\partial t} &= -[\frac{1}{2m}(\nabla S)^2 + V - \frac{\hbar^2}{2m}\frac{\nabla^2 R}{R}]\end{aligned} \tag{2.62}$$

The first equation defines the dynamics of the wave amplitude and may be rewritten as the continuity equation. The second equation can be viewed as an analogy to the classical Hamilton-Jacobi equation but with an extra term of 'quantum potential' $\frac{\hbar^2}{2m}\frac{\nabla^2 R}{R}$. The quantum potential relies on the information of the wave-function. In the classical limit, if we set $\hbar = 0$, the quantum potential is quenched.

Limitation exists for applying this quantum potential to general systems: there is one inverse of the amplitude$(1/R)$ in the quantum potential. To date, the Bohmian methodology has not found adequate solutions to handle the numerical problem [33].

An effective potential is also adopted by Centroid Molecular Dynamics [15] and is applied to the centroid path. Liu and Miller also proposed a version of an effective potential in the phase space [34] that goes beyond the Classical Wigner model. From ETMD [35], the trajectories are coupled with each other via an effective force, the effective force is similar to the quantum potential of Bohm. In the following chapters, I will first discuss an effective quantum force

based on the Classical Wigner model. And then I will also introduce a quantum force derived from the quantum Liouville equation. The effective forces (potentials) proposed by us aim at a reasonable accuracy, low numerical cost and also a clear physical insight.

# Chapter 3

# Classical Wigner model with an effective quantum force

In section 2.6 of the previous chapter, I briefly introduced the Classical Wigner model. The Classical Wigner model is based on one approximation, viz. that the distance between the pair of Feynman paths in fig. 2.1 is close to zero. Such approximation will be valid for high temperature or heavy mass. The combination of quantum initial conditions plus classical dynamics makes CW one of the most outstanding semi-classical methods to deal with multi-dimensional applications.

However, the dynamical quantum effects will be quenched in the CW model [17] such as tunneling and interference.

In this chapter I am going to improve the CW model by approximately including dynamical quantum effects. I will introduce a delocalization parameter to represent the dynamical quantum effects. Then this parameter will be utilized to construct a quantum force. Towards multi-dimensional applications, a two-dimensional $H + H_2$ collinear reaction will be studied in the last section of this chapter.

## 3.1 The Classical Wigner model with an effective quantum force using a position independent delocalization parameter

In this section, I am going to introduce an improvement upon the classical force that the CW model utilizes. It was derived in paper I for the case of a flux-flux correlation function. Hence, from eq. (2.45) we substitute the $\hat{A}$ and $\hat{B}$ in eq. (2.47) to be $\hat{F}(\beta/2)$. From fig. 2.1, we get fig. 3.1 to present the flux-flux correlation function. Since the CW model is based on eq. (2.52) which assumes the characteristic distance between pair of paths to be zero, no dynamical quantum effects will be captured [17]. Instead, we approximate $\Delta x$s to be a characteristic value ($\eta_0$), which is the characteristic distance between pair of Feynman paths in fig. 3.1. The dynamical quantum effects are reflected by $\eta_0$. Since $\eta_0$ presents also the delocalization perspective of the mean path (classical path), I refer to it as a delocalization parameter in the following part of this thesis.

Now the question will be how to obtain the $\eta_0$? We suggest the $\eta_0$ as the value that contributes most to the initial matrix element $< x_i|\hat{F}(\beta/2)|x_i' >$ in fig. (3.1). An example is given in fig. 3.2 to illustrate the way to define the $\eta_0$.

Following eq. (2.52), one can use an effective force (named $f^{eff}$) to approximate the

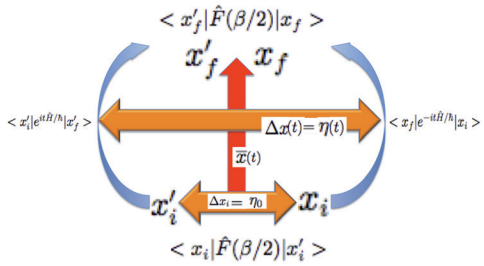


Figure 3.1: Two Feynman Paths generated from eq. (2.45) and eq. (2.47). The blue arrows specify the Feynman paths. The red arrow is the mean path (classical path) and the orange double arrows stand for the distances between two Feynman paths.

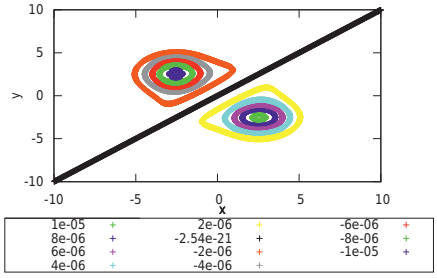


Figure 3.2: Two extrema $(2.55, -2.55), (-2.55, 2.55)$ are seen from this picture of the matrix element $< x|\hat{F}(\beta/2)|y >$ with $\beta = 12$ for a symmetric Eckart barrier ($V(x) = b/cosh^2(c * x)$, $cosh(cx) = 0.5(exp(cx) + exp(-cx))$, $m = \hbar = \omega^\sharp = 1$, $b = 6/\pi$, $c = \sqrt{\pi/12}$). $x$ and $y$ specifies different positions in the one-dimensional position coordinates. The $\eta_0$ value can be calculated as: $\eta_0 = 2.55 - (-2.55) = 5.1$

potential difference as $V(x_i) - V(x'_i) = -f^{eff}(\frac{x_i+x'_i}{2})(x_i - x'_i)$. We transform $x_i$ and $x'_i$ to the mean-difference coordinates of $q = \frac{x_i+x'_i}{2}$, $\eta = x_i - x'_i$. Then we substitute a characteristic value $\eta_0$ for all $\eta$s to obtain the effective force for position $q$:

$$f^{eff}(q) = \frac{V(q - \eta_0/2) - V(q + \eta_0/2)}{\eta_0}. \tag{3.1}$$

The two points to linearize the potential difference are separated by $\eta_0$. One can plot the true potential difference $V(q + \eta/2) - V(q - \eta/2)$ and the linearized potential difference $-f^{eff}(q) \times \eta$ for a fixed position $q$ for different $\eta$ values. They should match at $\eta = \eta_0$ where the matrix element is at its extremum. This is seen in fig. 3.3 for a symmetric Eckart barrier (the same potential as defined in fig. 3.2). The linearized potential difference agrees with the true potential difference at $\eta_0$.

The characteristic distance is position-independent (q-independent) in this section. A position dependent method will be addressed in the next section.

The effective potentials and the classical potential for a symmetric Eckart barrier (the

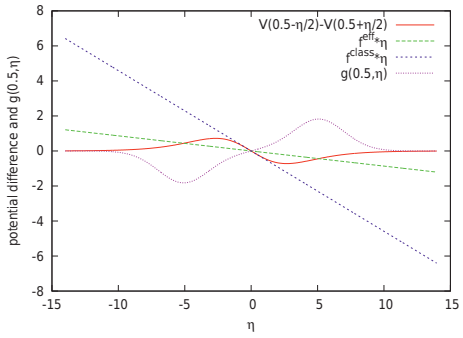


Figure 3.3: For $\beta = 12$ and $q = 0.5$, the linearized potential difference using both classical and quantum forces, the true potential difference and the matrix elements $g(0.5, \eta) =< 0.5 + \eta/2|\hat{F}(\beta/2)|0.5 - \eta/2 >$ for different $\eta$ values. The matching value of $\eta$ is $\eta = \eta_0 = 5.1$.

same potential as defined in fig. 3.2) at different temperatures are plotted in fig. 3.4. The barrier height of the effective potential is reduced as the temperature decreases.

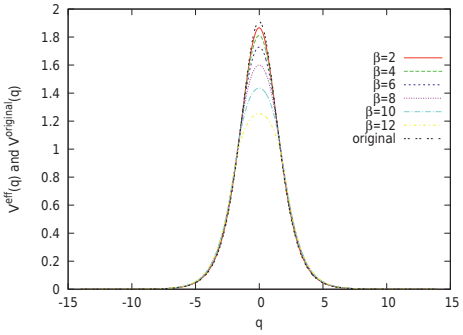


Figure 3.4: Effective and the classical potentials for a symmetric Eckart barrier at different $\beta = 1/k_B T$.

**Some results from application**

The flux-flux correlation functions from different methods at temperature $\beta = 1/k_B T = 12$ for a symmetric Eckart barrier (same potential as in fig. 3.2) is plotted in fig. 3.5.

The results of the transmission coefficient ($\kappa$) from CWEQF and the CW model are presented in Table. 3.1. Accurate $\kappa$ values are taken from [36].

**Table 3.1**. Transmission coefficients for a symmetric Eckart barrier (the same potential as in fig. 3.2).

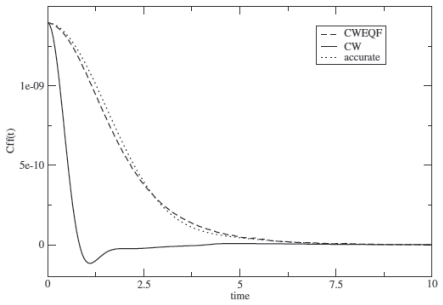


Figure 3.5: Flux-flux correlation functions from CW, CWEQF and exact reaults for a symmetric Eckart potential at $\beta = 1/k_B T = 12$.

| $\beta = 1/k_B T$ | 2 | 4 | 6 | 8 | 10 | 12 |
|---|---|---|---|---|---|---|
| $\kappa$(CW) | 1.14 | 1.7 | 3.2 | 9.4 | 46 | 360 |
| $\kappa$(CWEQF) | 1.16 | 1.8 | 4.6 | 19.8 | 152 | 1900 |
| $\kappa$(Accurate) | 1.22 | 2.07 | 5.2 | 21.8 | 162 | 1970 |
| $\eta_0$ | 1.1 | 1.7 | 2.5 | 3.3 | 4.2 | 5.1 |

From fig. 3.5 and Table. 3.1, it is seen that the CWEQF improves the CW model in a wide temperature range. Also the numerical cost of CWEQF equals to the CW model except for a search of the extrema at the initial time step. However, this is trivial compared to the cost of constructing the matrix elements. So we can conclude that the CPU demand of the CWEQF compared to the CW model increases only slightly.

## 3.2 The CWEQF using position dependent characteristic delocalization parameters

An effective quantum force is derived in the previous section with a position-independent delocalization parameter. The quantum force improves the original CW model.

However, a single delocalization parameter in the whole space does not entirely fit into our physical concept. From Martens et al, [37–39], the quantum correction (compared with the classical force) should be connected with the local Wigner function. Such worries reflect in the numerical application, too. For an asymmetric barrier application ($V(q) = a/(1 + \exp(-2q/c)) + b/cosh^2(q/c)$, $a = -18/\pi$, $b = 13.5/\pi$, $c = 8/\sqrt{3\pi}$, $m = \hbar = \omega^\sharp = 1$) with temperature below $\beta = 6$ , there will be two pairs of extrema in the matrix elements. It challenges the mechanism of using single value of $\eta_0$. Furthermore, even in the symmetric Eckart barrier applications, if one chooses a position $q$ some distance away from the dividing surface (for example $q = q_{ds} + 1.8$) and makes the corresponding plot as in fig. 3.3, then one will arrive at fig. 3.6. The true potential difference and the linearized one does not meet at $\eta_0$ which is obtained from the matrix elements.

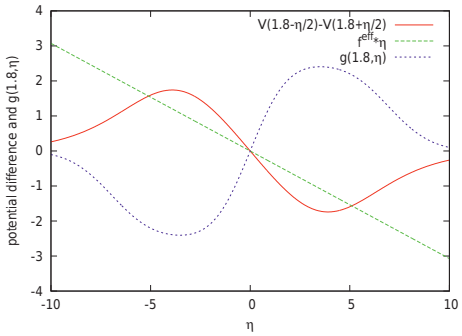


Figure 3.6: The diagram shows for $\beta = 12$ and $q = 1.8$, the linearized potential difference with the quantum force (with position-independent $\eta_0$), the true potential difference and the matrix element $g(1.8, \eta) =< q + \eta/2|\hat{F}(\beta/2)|q - \eta/2 >$ for different $\eta$ values. The point of the matching from the position independent determination of $\eta$ is $\eta = 5.1$. The matrix element is at its peak when $\eta$=3.6.

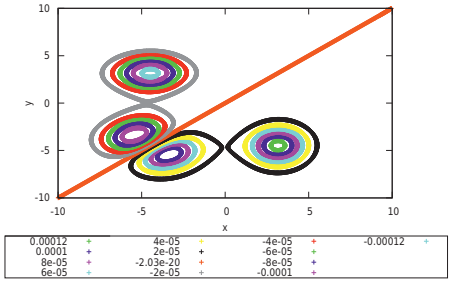


Figure 3.7: Two pairs of extrema for the matrix elements $< x|\hat{F}(\beta/2)|y >$ of an asymmetric Eckart barrier at $\beta = 12$.

Under such circumstances, the CWEQF with a position independent $\eta_0$ is not the optimized choice. In paper I, for an asymmetric barrier at low temperature, the matrix elements (see fig. 3.7) contain two pairs of extrema instead of only one pair. Each pair specifies a value of $\eta_0$. Then we split the Wigner function into two different parts, each with a different $\eta_0$ value.

If a trajectory moves between the two different parts in the Wigner space, we define the $\eta_0$ value to be the average of the $\eta_0$ values that belong to the different parts.

The results from this two-component model are satisfying and are presented in Table. 3.2.

**Table 3.2**. Transmission coefficients based on two-component model for an asymmetric Eckart barrier.

| $\beta = 1/k_B T$ | 8 | 10 | 12 |
|---|---|---|---|
| $\kappa$(CW) | 21 | 375 | 29000 |
| $\kappa$(CWEQF(with two characteristic $\eta_0$)) | 24 | 250 | 6800 |
| $\kappa$(Accurate) | 26 | 250 | 4100 |
| $\eta_0$ | 2.02,4.85 | 1.96,6.44 | 2.06,7.64 |

However, the two-component method is not ready to be applied to general potentials because sometimes the boundary of two regions will be blurred thus it is arbitrary to divide the phase space. The next task will be to overcome such problem and prepare the CWEQF for general potentials. The effective force is thus

$$f^{eff}(q) = \frac{V(q - \frac{\eta_0(q)}{2}) - V(q + \frac{\eta_0(q)}{2})}{\eta_0(q)}. \tag{3.2}$$

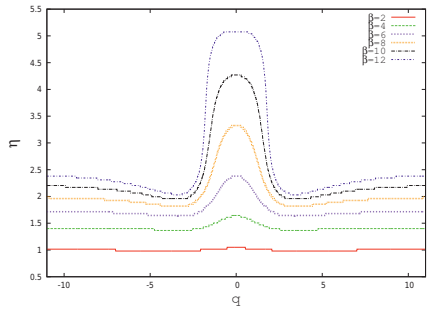


Figure 3.8: $\eta_0(q)$ for a symmetric Eckart barrier

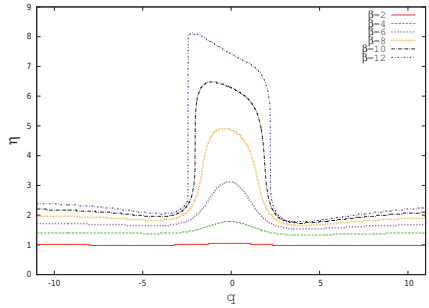


Figure 3.9: $\eta_0(q)$ for an asymmetric Eckart barrier

The value of $\eta_0(q)$ reflects the delocalization effects for different positions. The $\eta_0(q)$ for a symmetric and an asymmetric Eckart barrier for different temperatures is shown in fig. 3.8 and fig. 3.9 respectively.

Now we use the quantum force in eq. (3.2) to get the linearized potential difference. In fig. 3.10, we compare the linearized potential difference with the true potential difference for $q = 1.8$. It is seen that the position where the true potential difference meets the linearized potential difference agrees with the extrema of the matrix element. The advantage of using position dependent $\eta_0$ is obvious: it can be applied to potentials which contain more than one pair of extrema.

**Some results from applications**

**Table 3.3**. Transmission coefficients for a symmetric Eckart barrier potential (same potential as in Table 3.1) obtained using position-dependent $\eta_0$ values.

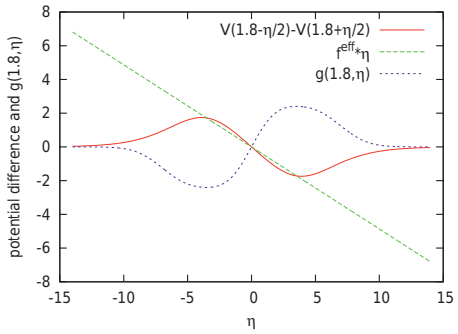


Figure 3.10: The figure shows (for $\beta = 12$ and $q = 1.8$): the linearized potential difference using the quantum force (with position dependent $\eta_0$), the true potential difference and the matrix element $g(1.8.\eta) =< 1.8 + \eta/2|\hat{F}(\beta/2)|1.8 - \eta/2 >$ for different $\eta$ values. The matching between the true and linearized potential difference occurs for $\eta = 3.6$. Such $\eta$ value also corresponds to the extrema of the matrix element.

| $\beta$ | 2 | 4 | 6 | 8 | 10 | 12 |
|---|---|---|---|---|---|---|
| $\kappa$ (CWEQF ($\eta_0(q)$)) | 1.16 | 1.82 | 4.38 | 19 | 149 | 1846 |
| $\kappa$ (CWEQF ($\eta_0$)) | 1.16 | 1.8 | 4.6 | 20 | 150 | 1890 |
| $\kappa$ (Exact) | 1.19 | 2.03 | 5.1 | 21.4 | 158 | 1935 |
| $\kappa$ (CW) | 1.15 | 1.7 | 3.3 | 9.9 | 49 | 398 |

**Table 3.4**. Transmission Coefficients for an asymmetric Eckart barrier potential (same potential as in Table 3.2) obtained using position-dependent $\eta_0$ values.

| $\beta$ | 2 | 4 | 6 | 8 | 10 | 12 |
|---|---|---|---|---|---|---|
| $\kappa$ (CWEQF ($\eta_0(q)$)) | 1.17 | 1.92 | 5.05 | 23.5 | 172 | 3646 |
| $\kappa$ (CWEQF ($\eta_0$)) | 1.17 | 1.9 | 5.4 | 24 | 250 | 6800 |
| $\kappa$ (Exact) | 1.2 | 2.0 | 5.3 | 26 | 250 | 4100 |
| $\kappa$ (CW) | 1.16 | 1.8 | 4.1 | 21 | 374 | 29300 |

We can conclude that the CWEQF with position-dependent $\eta_0$ works consistently better than the CW model. Since one does not have to divide the phase space into different parts, the CWEQF with position dependent delocalization parameter can be applied to general potentials.

## 3.3 CWEQF for two dimensional calculations

The previous sections set up the CWEQF model in one-dimension which works consistently better than the CW model. The next task is to generalize our CWEQF to larger dimensional applications. We will apply the CWEQF method to the two dimensional benchmark $H_A + H_B H_C = H_A H_B + H_C$ collinear reaction in this section. Both the CW method (by using the flux-side correlation function [40]) and the quantum-transition-state-theory (QTST) [41] applied to this problem over-estimated the rate constant by more than three times at 200K. We use the symmetrized flux-flux correlation function based on eq. (2.44) and eq. (2.45) in this section to study the collinear hydrogen exchange reaction in two dimensions.

We specify the reaction coordinate $x$ and the corresponding orthogonal coordinate $y$ as [41]

$$x = \sqrt{\frac{1}{2}}(R_{BC} - R_{AB}),$$
$$y = \sqrt{\frac{1}{2}}(R_{AB} - R^{\ddagger}_{AB} + R_{BC} - R^{\ddagger}_{BC}), \tag{3.3}$$

where $R_{AB}$ and $R_{BC}$ are the bond distances between different hydrogen atoms. $(R^{\ddagger}_{AB}, R^{\ddagger}_{BC})$ specifies the saddle point positions. The product side is defined as $x > 0$, the reactant side is thus x<0. For collinear reaction, we have $R_{AC} = R_{AB} + R_{BC}$.
The Hamiltonian for this system is [41]

$$H = \frac{1}{2m_x}p_x^2 + \frac{1}{2m_y}p_y^2 + V(x,y),$$
$$m_x = m_H/3,$$
$$m_y = m_H. \tag{3.4}$$

Following Yamamoto [29], we get a symmetrized flux-flux correlation function for the two-dimensional case

$$C^{2d}_{ff}(t) = \frac{1}{(2\pi\hbar)^2}\int dp_x \int dx \int dp_y \int dy \times$$
$$F_w((\beta/2, x_{ds}); x(t), y(t), p_x(t), p_y(t)) F_w((\beta/2, x_{ds}); x(0), y(0), p_x(0), p_y(0))$$
$$. \tag{3.5}$$

The rate constant for the two dimensional calculation is thus

$$k^{2d}(T) = \frac{1}{Q_r(T)}\int_0^{\infty} dt C^{2d}_{ff}(t). \tag{3.6}$$

For the two-dimensional case, the $\eta_0$ values are two-dimensional vectors $\vec{\eta}_0 = (\eta_{x0}, \eta_{y0})$, which are shown in fig. 3.11. It is seen that along the Minimum Energy Path (MEP), the $\vec{\eta}_0$ vectors are aligned with it.

A difficulty arises when we construct the two dimensional effective quantum force. In the one dimensional case, we successfully constructed an effective quantum force which was as simple as the classical one. However, for the two-dimensional case, $\eta_0$ becomes a vector. For arbitrary $\vec{r} = (x, y)$ and $\vec{\eta} = (\eta_x, \eta_y)$, the problem is how to linearize the two dimensional potential difference surface $V(\vec{r} + \vec{\eta}/2) - V(\vec{r} - \vec{\eta}/2)$. Suppose we can get an effective force as we did in the one-dimensional applications and the effective force vector is $\vec{V}' = (V^{eff}_x, V^{eff}_y)$. To determine the two components, two equations are required. The first equation is obtained by linearizing the potential difference between the two extrema of the matrix elements $< x - \eta_x/2, y - \eta_y/2|\hat{F}(\beta/2)|x + \eta_x/2, y + \eta_y/2 >$, which follow the blue arrow in fig. 3.12.

$$\vec{V}' \cdot \vec{\eta}_0(\vec{r}) = V(\vec{r} - \frac{\vec{\eta}_0(\vec{r})}{2}) - V(\vec{r} + \frac{\vec{\eta}_0(\vec{r})}{2}), \tag{3.7}$$

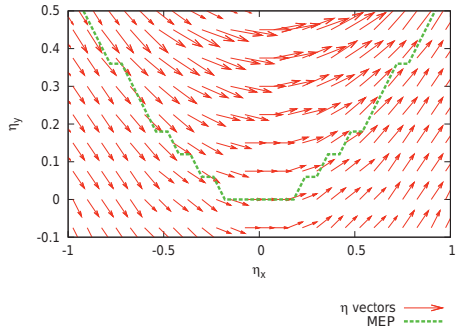


Figure 3.11: $(\eta_{x0}, \eta_{y0})$ for 2-dimensional potential

However, eq. (3.7) does not make the linear surface unique. It can be rotated around the axis of $\vec{\eta}_0$. We solve this problem by finding a pair of points along the orthogonal direction of $\vec{\eta}_0$. For each fixed $\vec{r}$, there is only one pair of extrema of the matrix elements when $(\eta_x, \eta_y)$ is varied. The characteristic distance in the orthogonal direction to $\vec{\eta}_0$ should be infinitesimally small. This means that we can choose a pair of points infinitesimally separated along the orthogonal direction to linearize the potential difference, as illustrated in fig. 3.12.

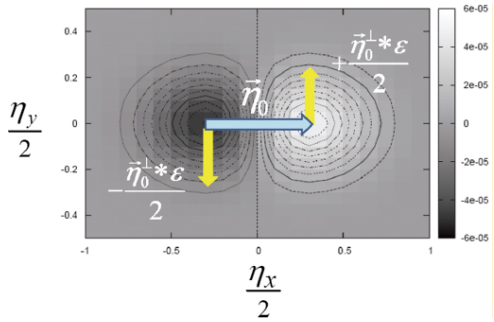


Figure 3.12: For $r_x = 0$, $r_y = 0.5$, we plot the matrix element of $< r_x - \eta_x/2, r_y - \eta_y/2|\hat{F}(\beta/2)|r_x + \eta_x/2, r_y + \eta_y/2 >$ for different $\eta_x$ and $\eta_y$ values. The beginning and ending points of the blue arrow represent the extrema of the matrix elements, thereby defining $\eta_{x0}$ and $\eta_{y0}$. The yellow vectors specify the infinitesimal movement along the orthogonal direction to $\vec{\eta}_0$. $T = 1000K$, $r_x = 0$, and $r_y = 0.5$.

This brings

$$\begin{pmatrix} V_x^{eff}(\vec{r}) \\ V_y^{eff}(\vec{r}) \end{pmatrix} \cdot (\vec{\eta}_0^{\perp} * \varepsilon + \vec{\eta}_0) =$$

$$V(\vec{r} + \vec{\eta}_0/2 + \vec{\eta}_0^{\perp} * \varepsilon/2) - V(\vec{r} - \vec{\eta}_0/2 - \vec{\eta}_0^{\perp} * \varepsilon/2). \tag{3.8}$$

Here we have $\varepsilon \to 0$ and $\vec{\eta}_0^{\perp} = (-\frac{\eta_{y0}}{\sqrt{(\eta_{x0})^2+(\eta_{y0})^2}}, \frac{\eta_{x0}}{\sqrt{(\eta_{x0})^2+(\eta_{y0})^2}})$ which is the unit vector in the direction orthogonal to $\vec{\eta}_0$. Combining eq. (3.7) and eq. (3.8), we get the solution:

$$f_x(x,y) = -\frac{(V(x+\eta_{x0}/2, y+\eta_{y0}/2) - V(x-\eta_{x0}/2, y-\eta_{y0}/2)) * \eta_{x0}}{(\eta_{x0})^2 + (\eta_{y0})^2} + \frac{0.5 \times (V'_y(x-\eta_{x0}/2, y-\eta_{y0}/2) + V'_y(x+\eta_{x0}/2, y+\eta_{y0}/2)) * \eta_{x0} * \eta_{y0}}{(\eta_{x0})^2 + (\eta_{y0})^2} - \frac{0.5 \times (V'_x(x-\eta_{x0}/2, y-\eta_{y0}/2) + V'_x(x+\eta_{x0}/2, y+\eta_{y0}/2)) * (\eta_{y0})^2}{(\eta_{x0})^2 + (\eta_{y0})^2}$$

$$f_y(x,y) = -\frac{(V(x+\eta_{x0}/2, y+\eta_{y0}/2) - V(x-\eta_{x0}/2, y-\eta_{y0}/2)) * \eta_{y0}}{(\eta_{x0})^2 + (\eta_{y0})^2} - \frac{0.5 \times (V'_y(x-\eta_{x0}/2, y-\eta_{y0}/2) + V'_y(x+\eta_{x0}/2, y+\eta_{y0}/2)) * (\eta_{x0})^2}{(\eta_{x0})^2 + (\eta_{y0})^2} + \frac{0.5 \times (V'_x(x-\eta_{x0}/2, y-\eta_{y0}/2) + V'_x(x+\eta_{x0}/2, y+\eta_{y0}/2)) * \eta_{y0} * \eta_{x0}}{(\eta_{x0})^2 + (\eta_{y0})^2}. \quad (3.9)$$

This choice is however not guaranteed to be optimal. There may be more accurate ways to choose the second equation, rather than approximating the delocalization parameter along the orthogonal direction to be the thermal de Broglie wavelength.

**Some results from application**

The two-dimensional results for the collinear $H + H_2$ reaction are shown in Fig. 3.13 and Fig. 3.14.

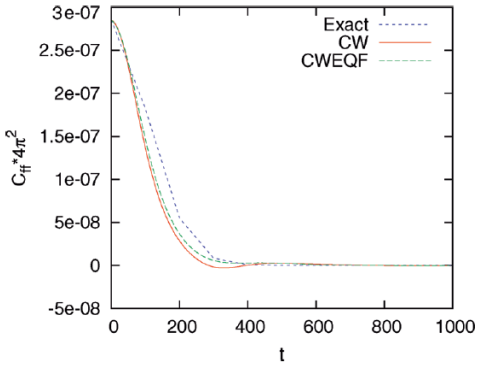


Figure 3.13: Comparison of an accurate $C_{ff}$ with those for the CW and CWEQF models at $1000\ K$. Time is in atomic unites.

We can conclude that the CWEQF works consistently better compared with the CW model.

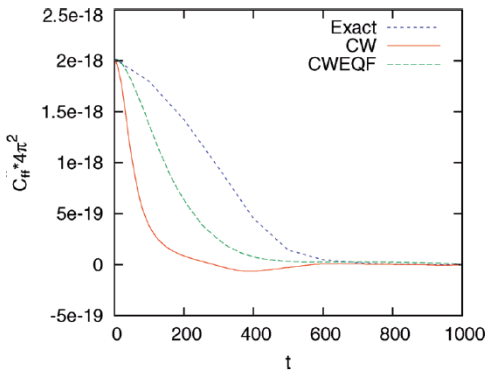


Figure 3.14: Comparison of an accurate $C_{ff}$ with those for the CW and CWEQF models at 200 $K$. Time is in atomic units.

# Chapter 4

# A deeper insight into the tunneling regime

## 4.1 Entangled Trajectory Molecular Dynamics

The previous chapter initiated the idea about using the delocalization parameter to linearize the potential difference as an effective quantum force. We studied a canonical system (in the NVT ensemble) in the CWEQF method where temperature becomes important to determine the delocalization parameter. However, we want to extend our idea of the quantum potential to general systems, like micro-canonical systems of well-defined energy $E$ for example. In this chapter, I am going to present the dynamics of particles under quantum Liouville equation in a semi-classical way. I will first introduce a method named Entangled Trajectory Molecular Dynamics (ETMD). The force for each trajectory is generated from the entanglements between the trajectories. Then I will present our effective force based on ETMD to propagate the trajectories. In the end, I will show the application of our effective force in two-dimensional applications.

Many trajectory-based methods have been invented to run classical-like trajectories dressed with quantum effects [15, 19, 26, 30, 31, 35, 37, 38, 42–51]. The method we present here is based on the Wigner distribution function [25] which is described in chapter 2. From eq. (2.24), the Wigner function corresponding to the density operator $\hat{\rho}(t)$ is

$$\rho^W(q,p,t) = \frac{1}{2\pi\hbar}\int < q+y/2|\hat{\rho}(t)|q-y/2 > e^{ipy/\hbar}dy, \tag{4.1}$$

with $q$ and $p$ being the position and momentum coordinates. $y$ is related to the off-diagonal elements $< q+y/2|\hat{\rho}|q-y/2 >$ (this $y$ is not to be confused with the one in section 3.3). In the following, I will briefly introduce the derivation of the ETMD's equations of motion [26]. From [26], the time evolution of the Wigner function follows

$$\frac{\partial\rho^W(q,p,t)}{\partial t} = -\frac{p}{m}\frac{\partial\rho^W(q,p;t)}{\partial q} + \int J(q,\xi-p)\rho^W(q,\xi,t)d\xi, \tag{4.2}$$

where

$$J(q,\xi) = \frac{i}{2\pi\hbar^2}\int [V(q+z/2)-V(q-z/2)]e^{-iz\xi/\hbar}dz. \tag{4.3}$$

Now we introduce the continuity equation as follows:

$$\frac{\partial\rho^W(q,p,t)}{\partial t} = -\vec{\nabla}\cdot\vec{j}, \tag{4.4}$$

where $\vec{j}$=$(j_q, j_p) = (\dot{q}\rho^W(q,p,t), \dot{p}\rho^W(q,p,t))$ shows the current vector in phase space, $\dot{q}$ represents the velocity and $\dot{p}$ denotes the force. $\vec{\nabla} = (\partial/\partial q, \partial/\partial p)$ is the phase space gradient

operator. Combining eq. (4.2) and eq. (4.4), one obtains:

$$\vec{\nabla} \cdot \vec{j} = \frac{p}{m} \frac{\partial \rho^W(q,p,t)}{\partial q} - \int J(q, \xi - p) \rho^W(q, \xi, t) d\xi. \tag{4.5}$$

$$j_q = \rho^W \dot{q} = \frac{p}{m} \rho^W \tag{4.6}$$

$\dot{q} = \frac{p}{m}$ is the velocity of the trajectory. The second component of eq. (4.5) is thus

$$\frac{\partial}{\partial p} j_p = - \int J(q, \xi - p) \rho^W(q, \xi, t) d\xi. \tag{4.7}$$

By integrating eq. (4.7) over $p$ from both sides we get

$$j_p = - \int \Theta_k(q, \xi - p) \rho^W(q, \xi, t) d\xi. \tag{4.8}$$

where

$$\Theta(q, p - \xi) = \frac{1}{2\pi\hbar} \int \frac{V(q + y/2) - V(q - y/2)}{y} \exp\left[-i \frac{(p - \xi)y}{\hbar}\right] dy. \tag{4.9}$$

So

$$\dot{p} = ma = j_p / \rho^W = \frac{1}{\rho^W(q,p)} \int \Theta(q, p - \xi) \rho^W(q, \xi) d\xi. \tag{4.10}$$

where $\dot{p}$ denotes the force. Combining eq. (4.9) and eq. (4.10) together, we get

$$\dot{p} = \frac{1}{\rho^W(q,p)} \int dy \frac{V(q + y/2) - V(q - y/2)}{y} \exp\left[-i \frac{py}{\hbar}\right] \frac{1}{2\pi\hbar} \int d\xi \exp\left[i \frac{y\xi}{\hbar}\right] \rho^W(q, \xi, t) \tag{4.11}$$

From eq. (4.11), for different momenta $\xi$, $\rho^W(q, \xi, t)$ presents different phase space points at the same position and the integration of $y$ evaluates all possible positions. One can see that the force of certain trajectory entangles with the other trajectories in phase space. The method thus bears the name of entangled trajectory molecular dynamics (ETMD) [38]. The ETMD method has been applied to several model potentials and is able to yield reaction probabilities in good agreement with exact results [26, 35].

The ETMD method also brings vivid explanation to the tunneling mechanism: the trajectories borrow energy from each other via entanglements to pass the potential barrier. Once the trajectories land on the other side of the dividing surface, they will release the borrowed energy. Thus forms a vivid picture to explain the tunneling mechanism [37, 38].

However, this explanation needs to be more qualitatively especially quantitatively specified, such as the physical correspondence of 'borrowing'. Furthermore, to calculate the ETMD force for a point in phase space there are two integrations to carry out, which might be numerically expensive. From eq. (4.11), the force diverges when $\rho^W(q,p,t) \to 0$ so there might be problems in regions where the Wigner function changes sign. The latter problem might be overcome by introducing the Husimi representation whereby no negative regions remain as a result of averaging over regions by a Gaussian function [39, 52]. However, the dynamics become more complicated to generalize for arbitrary potentials. Also, to reduce the numerical cost, one has to find a good approximation to substitute for the entanglements in the ETMD force.

## 4.2 Substitution for the entanglement by an effective force

I briefly introduced the ETMD method in the previous section. The ETMD method is able to capture the dynamical quantum effect through entanglements between trajectories. However, there is still room left for making it more practical. We aim at a delocalization parameter as we did in chapter 3 to generate an effective quantum force to substitute for the entanglements.

In eq. (4.11), the integration over $\xi$ is the inverse Fourier transform of the Wigner function which is defined in eq. (4.1). Thus

$$\dot{p} = \frac{1}{\rho^W(q,p)} \int dy \frac{V(q+y/2) - V(q-y/2)}{y} \times \exp\left[-i\frac{py}{\hbar}\right] < q+y/2|\hat{\rho}|q-y/2 > . \tag{4.12}$$

First, assume that the characteristic value of $y$ in eq. (4.12) is close to zero. We can then Taylor expand the potential difference to obtain $V(q+y/2)-V(q-y/2) \approx V'(q)y$. The force becomes

$$\dot{p} = \frac{-V'(q)}{\rho^W(q,p)} \times \int dy \exp\left[-i\frac{py}{\hbar}\right] < q+y/2|\hat{\rho}|q-y/2 > = -V'(q). \tag{4.13}$$

The ETMD model thus reduces to the ordinary CW model [20–22] which uses the classical force to propagate trajectories in Wigner space. The entanglements between the trajectories are thus removed. To go beyond the CW model, we assume here that a characteristic value $y_0(q)$ exists (the derivation will be shown in the next sections, also I use $y_0$ instead of $\eta_0$ here to distinguish the delocalization parameter of a NVT system and NVE system). This gives

$$\frac{V(q+y/2) - V(q-y/2)}{y} = \frac{V(q+y_0(q)/2) - V(q-y_0(q)/2)}{y_0(q)}. \tag{4.14}$$

The force in eq. (4.12) becomes

$$\dot{p} = -\frac{V(q+y_0(q)/2) - V(q-y_0(q)/2)}{y_0(q)}, \tag{4.15}$$

This force is much simpler than the ETMD force. It works in the same way as the CWE-QF's quantum force. The delocalization parameter becomes crucial in obtaining the dynamical quantum effects, it can be seen as a parameter that corresponds to the entanglements between trajectories. The next question is how to obtain such parameter.

## 4.3 The way to define the $y_0$

In the previous section, I introduced the possibility to use an effective force to substitute for the ETMD force. However, we need to define the delocalization parameter ($y_0$) to construct

the effective quantum force.

In previous chapter, we define the delocalization parameter corresponding to the extrema from the matrix elements of $< q+\eta/2|\widehat{F}(\beta/2)|q-\eta/2 >$. The present work concerns the density operator rather than the thermal flux operator. Take the Gaussian wave packet for example [26]: from eq. (2.30), the extrema of the density matrix elements are along the diagonal line $(\eta = 0)$, so a different way to determine the delocalization parameter is needed.

From the work of ETMD [26, 35, 37–39], the particle is always prepared as a Gaussian wave packet to propagate (see eq. (2.27)). Thus the Wigner function initially is expressed as a Gaussian (see eq. (2.28)). The delocalization parameter is assumed to be the width of the Gaussian ($y_0 = \sigma_q$) in position coordinate. From eq. (2.28), the width of the position and momentum of the Gaussian satisfies the minimum uncertainty relation: $\sigma_q\sigma_p = \hbar/2$. As time goes on, let's simply assume that the Wigner function still conserves such minimum uncertainty. Thus for different position q: $y_0(q) = \Delta_q(q) = 0.5\hbar/\Delta_p(q)$ (where $\Delta_q(q)$ and $\Delta_p(q)$ specify the square roots of the variances along position and momentum coordinates).

We are also aware that the smallest phase space area compatible with the uncertainty principle is named a quantum blob [53]. For a Gaussian distribution function, the quantum blob has an area of $\hbar/2$ which is consistent with the minimum uncertainty principle. We can update $\Delta_q(q)$ by calculating the variance of the momentum at an arbitrary position $q$. We use the above discussion as the motivation for our calculation of $y_0$. The square root of the variance of the momentum ($\Delta_p$) is:

$$\begin{aligned}\Delta_p &= (\overline{p^2} - (\overline{p})^2)^{\frac{1}{2}} \\ \overline{p} &= \int dp\rho^W(q,p,t)p/\int dp\rho^W(q,p,t) \\ \overline{p^2} &= \int dp\rho^W(q,p,t)p^2/\int dp\rho^W(q,p,t).\end{aligned} \tag{4.16}$$

The force generated in the ETMD method describes 'non-local' contributions via entanglement. In the present work, the entanglements between the trajectories will be absorbed into the parameter $y_0(q)$, which is defined by the distribution of momentum.

## 4.4 Another way of obtaining the $y_0$

If this section, we introduce another way to obtain the delocalization parameter. From the CWEQF method, we obtain an effective quantum force by using the characteristic distance between pair of Feynman paths that enters the expression of the thermal flux-flux correlation function ($C_{ff}$).

For an arbitrary operator $\hat{X}$ which is an operator only related to positions (such as $\hat{h}(\hat{x})$). The corresponding measurement of it at time t will be:

$$\begin{aligned}X(t) &= tr[\hat{\rho}\exp(-i\hat{H}t/\hbar)\hat{X}\exp(i\hat{H}t/\hbar)] \\ &= \int dxdx_1dx_2dx' < x|\hat{\rho}|x_1 >< x_1|\exp(-i\hat{H}t/\hbar)|x_2 > \\ &\quad < x_2|\hat{X}|x' >< x'|\exp(i\hat{H}t/\hbar)|x >\end{aligned} \tag{4.17}$$

From chapter 2 and chapter 3, we solve the trace via path integrals. Suppose the delocalization parameter is $y_\rho$ for the matrix element of $< x|\hat{\rho}|x_1 >$. The delocalization parameter for matrix

element $< x'|\hat{X}|x >$ is $y_X$. One thus gets an effective characteristic distance in eq. (4.17) following the average: $y_0^{effective} = 0.5 * (y_\rho + y_X)$. From paper I,

$$X(t) = \int dp \int dq \rho^w(p, q, t = 0) X(q_t) \tag{4.18}$$

For the matrix element of $< q+y/2|\hat{\rho}|q-y/2 >$, since the extrema are positioned at $\eta = 0$ (see eq. (2.30)), we assume the delocalization parameter of the density operator $\hat{\rho}$ to be $y_\rho(q)$ and that it equals to the width ($y_\rho^{width}$) of the distribution along $y$. We still approximate the shape of the Wigner function to be a Gaussian distribution [43, 54].

Now we come back to eq. (4.17), for position $q$, we have

$$y_0^{effective}(q) = 0.5(\eta_\rho^{width} + y_X). \tag{4.19}$$

Since $y_X = 0$, $y_0^{effective}(q)$ is half value of the geometric width of the off-diagonal distribution ($y_\rho^{width}$) of the matrix element $< q+y/2|\hat{\rho}|q-y/2 >$. From section (2.3), we have $y^{width} = 2\sigma_q$ for a Gaussian Wigner function thus $y_0^{effective}(q)$ is the same value as the delocalization parameter derived in the previous section.

**Some results from application**

We apply our effective quantum force to study the reaction probability for a cubic potential (fig. 4.1).

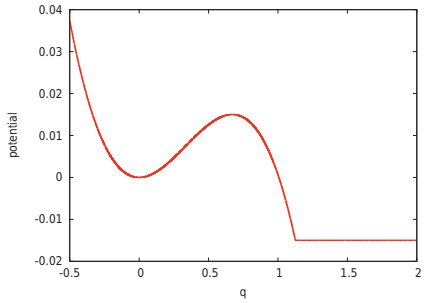


Figure 4.1: The cubic potential $V(q) = \frac{1}{2}m\omega_0^2 q^2 - \frac{1}{3}bq^3$, $\omega_0 = 0.01$, $b = 0.2981$, $m = 2000$. From [26], a cut-off value of $-0.015$ is adopted for $q > 1.12556$.

The initial wave function is centered in the potential well. One can refer to paper III for numerical details. The reaction probability (escape probability) is shown in fig. 4.2.

To explain such tunneling effects, we can focus on the dominant part of $y_0(q) = \hbar/2\Delta_p \approx \frac{0.5}{\sqrt{\overline{p^2}}}$. When the highest momentum trajectories pass over the barrier, the average kinetic energy (or $p^2$) will be reduced which will directly result in an increase of the characteristic delocalization parameter thus smear out the potential barrier to help the trajectories that have lower kinetic energy to cross over. The procedure will continue with time. This introduces one interesting phenomenon, the trajectories with less kinetic energy initially will have the chance to go over the potential barrier at later time. This forms a consistent explanation to the tunneling effect of the cubic potential where the reaction probability grows in time as shown in fig. 4.2. Such a mechanism is depicted in fig. 4.3.

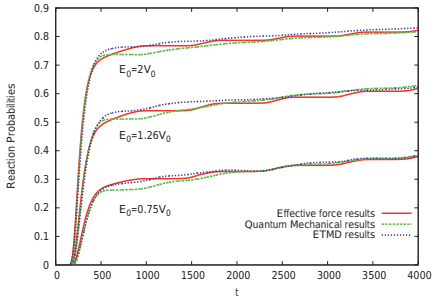


Figure 4.2: The reaction probability versus time for the cubic potential at three different average energies. The green curves are the exact results [26]. The red curves are the results obtained using our effective force constructed from the time-dependent delocalization parameters. The blue curves are the results of the ETMD method [26].

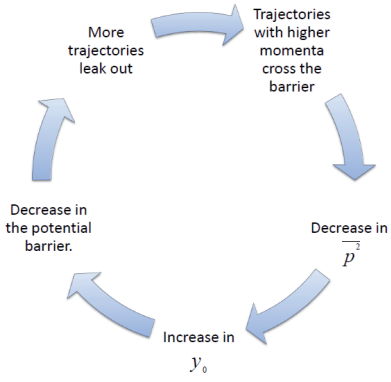


Figure 4.3: The explanation of the tunneling effect for the cubic potential in fig. 4.1.

## 4.5 Effective quantum force for two dimensional applications

In previous sections, we constructed an effective force to substitute for the entanglement between trajectories. Each trajectory is controlled by a quantum force which is updated in time. Now the challenge will be to generalize it to multi-dimensional applications. We are aware of that the ETMD method has been used to carry out two dimensional calculations and the results are inspiringly accurate compared with the exact ones [35]. It will be the task in this section to apply our quantum force to two dimensions. Since our method is close to the ETMD, I will start with a brief derivation of generalizing the ETMD to multi-dimensional applications from [35]. Then I will introduce our effective force based on this ETMD force.

For a multi-dimensional system consisting of particles with identical mass $m$ under a potential $V(q_1, ....q_n)$, the state of particles will be expressed by position vector $\vec{q} = (q_1...q_n)$ and momentum vector $\vec{p} = (p_1...p_n)$. The off-diagonal vector of matrix elements of $< \vec{q}+\vec{y}/2|\hat{\rho}|\vec{q}-\vec{y}/2 >$ is then a function of $\vec{y} = (y_1...y_n)$. The Wigner function of the multi-dimensional wave function $\Psi(\vec{q}, t)$ is

$$\rho^w(\vec{q}, \vec{p}, t) = \left(\frac{1}{2\pi\hbar}\right)^n \int \Psi^*(\vec{q}+\vec{y}/2, t)\Psi(\vec{q}-\vec{y}/2, t)e^{i\vec{p}\cdot\vec{y}/\hbar}d\vec{y}. \tag{4.20}$$

The time-evolution of this multi-dimensional Wigner function is then

$$\frac{\partial\rho^W(\vec{q}, \vec{p}, t)}{\partial t} = -\sum_{k=1}^{n}\frac{p_k}{m}\frac{\partial\rho^W(\vec{q}, \vec{p}; t)}{\partial q_k} + \int J(\vec{q}, \vec{\xi}-\vec{p})\rho^W(\vec{q}, \vec{\xi}, t)d\vec{\xi}, \tag{4.21}$$

where

$$J(\vec{q}, \vec{\xi}) = \frac{i}{2^n\pi^n\hbar^{n+1}}\int[V(\vec{q}+\vec{z}/2) - V(\vec{q}-\vec{z}/2)]e^{-i\vec{z}\cdot\vec{\xi}/\hbar}d\vec{z}. \tag{4.22}$$

Now we introduce the continuity equation as follows:

$$\frac{\partial\rho^W(\vec{q}, \vec{p}, t)}{\partial t} = -\vec{\nabla}\cdot\vec{j}, \tag{4.23}$$

where $\vec{j}$=$(j_{q1}...j_{qn}, j_{p1}...j_{pn}) = (\dot{\vec{q}}, \dot{\vec{p}})\rho^W(\vec{q}, \vec{p}, t)$ shows the current vector in phase space, $\dot{\vec{q}}$ presents the velocity and $\dot{\vec{p}}$ denotes the force. $\vec{\nabla} = (\partial/\partial q_1...\partial/\partial q_n, \partial/\partial p_1...\partial/\partial p_n)$ is the phase space gradient operator. Combining eq. (4.21) and eq. (4.23), we obtain:

$$\vec{\nabla}\cdot\vec{j} = \sum_{k=1}^{n}\frac{p_k}{m}\frac{\partial\rho^W(\vec{q}, \vec{p}, t)}{\partial q_k} - \int J(\vec{q}, \vec{\xi}-\vec{p})\rho^W(\vec{q}, \vec{\xi})d\vec{\xi} \tag{4.24}$$

To obtain each component of the current vector (especially the momentum vector), we adopt an approximation based on the work of Lifei et al [35]: the $k$th momentum flux is related to the delocalization from the $k$th position coordinate. Thus we define the corresponding $J_k$ as:

$$J_k(\vec{q}, \vec{\xi}) = \frac{i}{2^n\pi^n\hbar^{n+1}}\int[V_k^+ - V_k^-]e^{-i\vec{z}\cdot\vec{\xi}/\hbar}d\vec{z}, \tag{4.25}$$

where $V_k^{\pm} = V(q_1, ..q_k \pm y_k/2, ...q_n)$ and k=1,...n. From eq. (4.24) and eq. (4.25), the components of the current vector are

$$j_{qk} = v_{qk}\rho^W(\vec{q},\vec{p},t) = \frac{p_k}{m}\rho^W(\vec{q},\vec{p},t), \tag{4.26}$$

$$\frac{\partial}{\partial p_k} j_{pk} = -\int J_k(\vec{q},\vec{\xi}-\vec{p})\rho^W(\vec{q},\vec{\xi},t)d\vec{\xi}. \tag{4.27}$$

Integrating eq. (4.27) over $p_k$ on both sides we can get

$$j_{pk} = -\int \Theta_k(\vec{q},\vec{\xi}-\vec{p})\rho^W(\vec{q},\vec{\xi},t)d\vec{\xi}. \tag{4.28}$$

where

$$\Theta_k(\vec{q},\vec{p}-\vec{\xi}) = \frac{1}{2^n\pi^n\hbar^n}\int \frac{V_k^+ - V_k^-}{y_k}\exp[-i\frac{(\vec{p}-\vec{\xi})\cdot\vec{y}}{\hbar}]d\vec{y}. \tag{4.29}$$

So we get:

$$\dot{p_k} = ma_k = j_{pk}/\rho^W = \frac{1}{\rho^W(\vec{q},\vec{p})}\int \Theta_k(\vec{q},\vec{p}-\vec{\xi})\rho^W(\vec{q},\vec{\xi})d\vec{\xi}. \tag{4.30}$$

We then write the force as:

$$\dot{p_k} = ma_k = \frac{1}{\rho^W(\vec{q},\vec{p})}\int d\vec{y}\frac{V_k^+ - V_k^-}{y_k}\exp[-i\frac{\vec{p}\cdot\vec{y}}{\hbar}]\times \frac{1}{2^n\pi^n\hbar^n}\int d\vec{\xi}\exp[i\frac{\vec{y}\cdot\vec{\xi}}{\hbar}]\rho^W(\vec{q},\vec{\xi},t). \tag{4.31}$$

In our previous work, if we manage to find a characteristic value of $y_k^0(\vec{q})$, we will have

$$\begin{aligned}\dot{p_k} = ma_k &= \frac{1}{\rho^W(\vec{q},\vec{p})}\int d\vec{y}\frac{V_k^+ - V_k^-}{y_k}\times\exp[-i\frac{\vec{p}\cdot\vec{y}}{\hbar}] \\ &< q_1...q_k + y_k/2, ..q_n|\hat{\rho}|q_1, ...q_k - y_k/2, ...q_n >, \\ \dot{p_k} = ma_k &= -\frac{V_{0k}^+ - V_{0k}^-}{y_k^0(\vec{q})}\frac{\rho^W}{\rho^W} \\ &= -\frac{V_{0k}^+ - V_{0k}^-}{y_k^0(\vec{q})}.\end{aligned} \tag{4.32}$$

where $V_{0k}^{\pm} = V(q_1, ..., q_k \pm y_k^0/2, ..., q_n)$ and the $y_k^0(\vec{q})$ is defined as:

$$y_k^0(\vec{q}) = \Delta q_k = C\hbar/\Delta p_k. \tag{4.33}$$

where

$$\begin{aligned}\Delta p_k &= \sqrt{\overline{p_k^2} - (\overline{p_k})^2} \\ \overline{p_k} &= \int d\vec{p}\rho^W(\vec{q},\vec{p},t)p_k/\int d\vec{p}\rho^W(\vec{q},\vec{p},t) \\ \overline{p_k^2} &= \int d\vec{p}\rho^W(\vec{q},\vec{p},t)p_k^2\int d\vec{p}\rho^W(\vec{q},\vec{p},t).\end{aligned} \tag{4.34}$$

The value C is chosen to be 0.5 for Gaussian wave packets.

**Some results from applications**

The next step is to apply the effective quantum force to two different two-dimensional applications which are taken from [35]. The first one is a symmetric Eckart barrier plus a harmonic potential without coupling (Model I).

$$V(q_1, q_2) = V_a Sech^2(2q_1) + 0.5V_b q_2^2$$
$$Sech^2(2q_1) = 4/(\exp(2q_1) + \exp(-2q_1))^2 \tag{4.35}$$

where $V_a = 0.00625$, $V_b = 0.0106$, $m = 2000a.u$, $\omega = 0.004$. The mean energies are chose to be $E_0 = 0.85V_a$ and $E_0 = 1.12V_a$ for the particle. The results are presented in fig. 4.4.

The second model potential is a symmetric Eckart barrier plus a harmonic potential with coupling (Model II).

$$V(q_1, q_2) = V_a Sech^2(2q_1) + 0.5V_b[q_2 + V_c(q_1^2 - 1.0)]^2$$
$$Sech^2(2q_1) = 4/(\exp(2q_1) + \exp(-2q_1))^2 \tag{4.36}$$

where $V_a = 0.00625$, $V_b = 0.0106$, $m = 2000a.u$, $\omega = 0.004$. The mean energies are chosen to be $E_0 = 0.88V_a$ and $E_0 = 1.15V_a$. The results are shown in fig. 4.5.

We see good agreements between the exact results and the results from the quantum force for both applications. The quantum force in the NVE system works well in our two-dimensional applications.

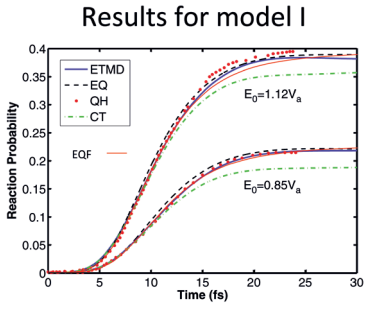


Figure 4.4: The reaction probability for different methods of calculation for model I. The Exact quantum mechanical results (EQ) are represented by the blue dashed lines, the red solid lines are the results from our quantum force (EQF). The results from quantum hydrodynamics (QH) [55] and ETMD results are shown as the red dotted lines and blue solid lines. The classical results (CT) are shown as the green lines.

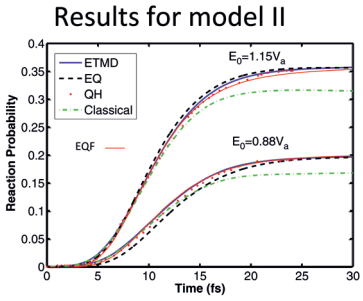


Figure 4.5: The reaction probability for different methods of calculation for model II. The Exact quantum mechanical results (EQ) are represented by the blue dashed lines, the red solid lines are the results from our quantum force (EQF). The results from quantum hydrodynamics (QH) [55] and ETMD results are shown as the red dotted lines and blue solid lines. The classical results (CT) are shown as the green lines.

# Chapter 5

# Summary and discussions

It was shown that dynamical quantum effects enter through a separation of paths in the Feynman Path Integral. This separation was represented by a delocalization parameter. We argued that by including its characteristic value in an effective quantum force, quantum effects could be included in molecular dynamics. In this chapter, I am going to briefly summarize the four papers included in this thesis.

In Paper I, we apply the Classical Wigner method with an effective quantum force (CWEQF) using a position independent delocalization parameter $\eta_0$ on two different one-dimensional potentials: a symmetric Eckart barrier and an asymmetric Eckart barrier. The results from the symmetric Eckart barrier are close to the exact ones over a wide range of temperatures. As for the asymmetric barrier at lower temperature, we encounter one problem, viz. that the matrix elements have two pairs of extrema instead of only one pair. We have to split the phase space into two different parts assigned different $\eta_0$ values. If a trajectory moves between the two different parts, the effective $\eta_0$ is chosen to be the average between the two $\eta_0$ values. By this method the results for the asymmetric Eckart barrier are inspiringly accurate. We use the initial matrix element to generate the parameter $\eta_0$ and keep it the same for all the time steps.

This works well for the applications in Paper I. The reason is that the potentials in Paper I contain only one single barrier and no potential wells to trap the trajectories. Thus the updating of dynamical quantum effect for a long time is not required.

Also, the effective potential from CWEQF is reduced to the classical form in the following limits:

(1) The classical limit: when $\hbar \to 0$, the value of the parameter $\eta_0$ reduces to zero in the same way as the thermal de Broglie wave length. This can also be deduced from the structure of the matrix elements plots like the one in fig. 3.2. When $\hbar$ goes to zero, the pair of extrema will approach the diagonal line. In this way, we obtain an infinitesimally small value of $\eta_0$ and a classical force.

(2) The harmonic limit: when the potential is quadratic, the effective force that CWEQF adopts is reduced to the classical force which is independent of the value of $\eta_0$ which is seen from the expression of the quantum force, $f^{eff}(q) = \frac{V(q-\eta_0/2)-V(q+\eta_0/2)}{\eta_0}$.

(3) The high temperature limit: when the temperature reaches the high temperature limit, the $\beta$ value reduces to an infinitesimally small value. The Bolzmann operator in the thermal-flux operator will become very narrowly-distributed (like a delta-function). Thus the off-diagonal elements in the matrix expression will be squeezed to the diagonal line, which brings an infinitesimal small value of the $\eta_0$. The classical force will also be obtained in the high temperature limit.

The comments above and the satisfying results of CWEQF make it possible to conclude that the quantum force obtained by using the characteristic delocalization parameter will pro-

duce a better-performed method compared with the CW method.

In Paper II, we try to improve the CWEQF via position-dependent $\eta_0$ values thus to obtain a consistent recipe for both symmetric and asymmetric Eckart barriers (without dividing the phase space into parts). Thus it can be applied to general potentials. Then we apply the CWEQF to a two-dimensional problem, which is the collinear $H + H_2$ reaction. However, the effective force is not as simple to construct as in the one dimensional case because we need two equations for the linearization of the potential difference. The first condition we find is to match the two points that are delocalized by the characteristic $\overrightarrow{\eta}_0$ vector, the second condition is to match the two points that are delocalized infinitesimally along the orthogonal direction to $\overrightarrow{\eta}_0$. The effective force we generate in this way produces consistently better results than the ordinary CW model.

However, we observe that the results for our two-dimensional application is still a distance away from the exact ones. The reason may be concluded to be as follows: the two dimensional potential can be treated as a symmetric Eckart barrier along the reaction coordinate plus a Morse potential in the orthogonal direction together with coupling between these two coordinates. Assuming that we treat the Morse potential approximately as a harmonic potential, the dynamics along this coordinate should be classical and independent of the other trajectories. So if we de-couple the two coordinates, the CW model and CWEQF model will both work much better. However, coupling does exist and functions in a nontrivial manner. Thus, how to treat the coupling between the coordinates during linearization will be challenging.

Based on the comments above, we conclude that the future improvement of the CWEQF should be focused on:

(1) A better linearization mechanism considering the multi-dimensional coupling.

(2) A method to update the delocalization vector in real-time under relatively low numerical cost.

In Paper III, we compare our effective force with the ETMD method for a micro-canonical system (NVE). We manage to derive our effective force by propagating the trajectories quasi-independently. The ETMD method is able to capture the essential quantum effects in the dynamics, which is the entanglement between different trajectories and is used to explain the tunneling dynamics. We try instead to use one parameter (the delocalization parameter $y_0$) to capture the entanglements.

To obtain the value of $y_0$, we resort to the minimum uncertainty principle. When the $y_0$ values are obtained, we propagate the trajectories independently under an effective force. However, it is not sound to say we propagate the trajectories independently of each other. Since all trajectories with the same position but different momenta are investigated to get the delocalization parameter, one can see that 'entanglements' exist between such trajectories. However, the delocalization parameter does not need the information from the other positions thus makes it less numerically demanding. Also the quantum force is momentum-independent which reduces the numerical cost even further.

There are three one-dimensional applications in Paper III: symmetric (asymmetric) Eckart barrier and the cubic potential. For the cubic potential, as time goes on, the delocalization parameter within the potential well becomes larger after the higher-momentum trajectories crossed

over the barrier. The barrier is hence decreased with time. We can see a quantum leak out effect for this kind of potential [26]. The results are as good as those of the ETMD method with numerical cost much reduced.

The quantum force obtained using our delocalization parameter in the NVE system has the following properties:

(1) The force will reduce to the classical force when we take the classical limit of $\hbar \to 0$. The uncertainty principle is quenched in this limit. So the delocalization parameter shrinks to zero thus resulting in a classical force.

(2) The quantum force will reduce to a classical force for quadratic potentials as shown in the discussion for the CWEQF above. The expression of the force is independent of the delocalization parameter under quadratic potentials thus classical force is always met.

(3) The delocalization parameter will reduce to zero in the high energy limit. In this limit, the variance of momentum will develop a large value thus squeeze the delocalization parameter to be close to zero. Then the classical force is obtained.

In Paper IV, we generalize our quasi-independent trajectory method to two dimensional problems. The calculation of the reaction probability we obtained yields good agreement with the results of the ETMD method. It is reasonable for us to predict good behavior in the first application which is a symmetric Eckart barrier plus a harmonic potential without coupling, since the dynamics along the orthogonal direction will be classical all the time. It is only along the reaction coordinate where quantum correction is needed. However, in the second application where we switch on the coupling between the two coordinates, the results are still accurate. The success of the second application thus indicates that the time dependence of the delocalization parameter will function compared with the method of CWEQF in two dimensional applications where the delocalization parameter is kept the same for all times. So a future work may be done for the collinear $H + H_2$ again by using a time-dependent strategy for the determination of the delocalization vectors.

The quantum force presents good behavior in two different ensembles (NVT and NVE for the systems). It retains the classical trajectories in the dynamics, however gains extra quantum correction to the dynamics. The future work will basically be focused on two aspects: first, a more strict derivation of the delocalization parameter for two different operators in the correlation function. Second, the real time up-dating of the delocalization parameter for the CWEQF method.

# Chapter 6

# Acknowledgments

I would like to thank:

My daughter Manting for the joyful company with me that brings continuous sunshine to me despite the windy and rainy weather.
My supervisors Gunnar Nyman and Jens Poulsen for their patience and help during my studies.
STINT foundation for offering me the scholarship to come and study in Sweden for my Master degree.
Rasmus Person for all the nice discussion about science and life.
Magnus Gustavson and Roland Kjellander for their guidance through the courses and project works.
Sture Nordholm for his nice lectures and social activities.
Shiwu Gao for his kind help in guiding me through my PhD studying.
Jan Franz, Huagen Yu and Dylan Drake-Wilhem for scientific discussion and all their help in scientific writing.
All my colleagues in the Physical Chemistry department for the accompany through the years.
Professor Yujun Zheng for his kind help in sharing his data with me to compare with and also the nice discussion with the dynamics in Phase space.
Eliza Cheng and all the secretaries that helped me during my studying period. All my friends that shared fun of football, ice hockey, and so on with me.

# Bibliography


[1] Allen, M. P.; Tildesley, D. J. *Computer Simulation of Liquids.* **1987**, New York: Oxford.

[2] Schulten, K. *In Simplicity and Complexity in Proteins and Nucleic Acids.* **1999**, Berlin: Dahlem Univ.

[3] Frenkel, D.; Smit, B. *Understanding Molecular Simulation.* **2001**, Academic Press.

[4] Chu, T. S.; Zhang, Y. ; Han, K. L. *INTERNATIONAL REVIEWS IN PHYSICAL CHEMISTRY.* **2006***, 25, 201*.

[5] Feit, M. D.; Fleck, J. A. J.; Steiger, S. A. *J. Comput. Phys.* **1982***, 47, 412*.

[6] Nyman, G.; Yu, H. G. *REPORTS ON PROGRESS IN PHYSICS.* **2000***, 63, 1001*.

[7] Nyman, G.; Yu, H. G. *INTERNATIONAL REVIEWS IN PHYSICAL CHEMISTRY.* **2013***, 32, 39*.

[8] Billing, G. D. *The Quantum-Classical Theory.* **2002**, Oxford University Press.

[9] Berne, B. J.; Ciccotti, G.; Coker, D. F. *Quantum and Classical Dynamics in Condensed Phase Simulations.* **1998**, Singapore: World Sci.

[10] Miller, W. H. *J. Phys. Chem. A.* **2001***, 105, 2942*.

[11] Thoss, M.; Wang, H. *Annu. Rev. Phys. Chem.* **2004***, 55, 299*.

[12] Miller, W. H. *J. Chem. Phys.* **1970***, 53, 3578*.

[13] Cao, J.; Voth, G. A.*J. Chem. Phys.* **1996***. 104, 273*.

[14] Makri, N.; Thompson, K. *Chem. Phys. Lett.* **1998***, 291, 101*.

[15] Cao, J.; Voth, G. A. *J. Chem. Phys.* **1994***, 100, 5106*.

[16] Miller, T. F.; Manolopoulos, D. E. *J. Chem. Phys.* **2005***, 122, 184503*.

[17] Miller, W. H. *J. Phys. Chem. A.* **2001***, 105, 2942*.

[18] Poulsen, J. A.; Nyman, G.; Rossky, P. J. *J. Chem. Phys.* **2003***, 119, 12179*.

[19] Shi, Q.; Geva, E. *J. Chem. Phys.* **2004***, 121, 3393*.

[20] Wang, H.; Sun, X.; Miller, W. H. *J. Chem. Phys.* **1998***, 108, 9726*.

[21] Wang, H., Song, X.; Chandler, D.; Miller, W. H. *J. Chem. Phys.* **1999***, 110, 4828*.

[22] Sun, X.; Wang, H.; Miller, W. H. *J. Chem. Phys.* **1998***, 109, 4190*.

[23] Poulsen, J. A.; Nyman, G.; Rossky, P. J. *J. Chem. Theory Comput.* **2006***, 2, 1482*.

[24] Bransden, B. H.; Joachain, C. J. *Quantum Mechanics.* **2000**, Addison-Wesley.

[25] Wigner, E. *Phys. Rev.* **1932***, 40, 749*.

[26] Wang, A.; Zheng, Y. J.; Martens, C. C.; Ren, W. Y. *Phys. Chem. Chem. Phys.* **2009***, 11, 1588*.

[27] Zinn. Justin Jean. *Path Integrals in Quantum Mechanics,* **2004**, Oxford University Press.

[28] Makri, N.; Miller, W. H. *Chem. Phys. Lett.* **1988***, 151, 1*.

[29] Yamamoto, T. *J. Chem. Phys.* **2002***, 116, 7335*.

[30] Lopreore, C. L.; Wyatt, R. E. *Phys. Rev. Lett.* **1999***, 82, 5190*.

[31] Trahan, C. J.; Wyatt, R. E. *J. Chem. Phys.* **2003***, 119, 7017*.

[32] Bohm, D. *Phys. Rev.* **1952***, 85, 166*.

[33] Zhao, Y.; Makri, N. *J. Chem. Phys.* **2003***, 119, 1*.

[34] Liu, J. *J. Chem. Phys.* **2011***, 134, 194110*.

[35] Wang, L. F.; Martens, C.; Zheng, Y. J. *J. Chem. Phys.* **2012***, 137, 034113*.

[36] Shao, J.; Liao, J-L.; Pollak, E. *J. Chem. Phys.* **1998***, 108, 9711*.

[37] Donoso, A.; Zheng, Y. J.; Martens, C. C.. *J. Chem. Phys.* **2003***, 119, 5010*.

[38] Donoso, A.; Martens, C. C. *Phys. Rev. Lett.* **2001***, 87, 223202*.

[39] Lopez, H.; Martens, C. C.; Donoso, A. *J. Chem. Phys.* **2006***, 125, 154111*.

[40] Zheng, Y. J.; Pollak, E. *J. Chem. Phys.* **2001***, 114, 9741*.

[41] Liao, J-L.; Pollak, E. *J. Chem. Phys.* **1999***, 110, 80*.

[42] Miller, W. H. *J. Chemical. Phys.* **2006***, 125, 132305*.

[43] Heller, E. J. *J. Chem. Phys.* **1975***, 62, 1544*.

[44] Kelly, A.; Zon, R. V.; Schofield, J.; Kapral, R. *J. Chem. Phys.* **2012***, 136, 084101*.

[45] Garashchuk, S; Mazzuca, J; Vazhapilly, T. *J. Chem. Phys.* **2011***, 135, 034104*.

[46] Lopez, H.; Martens, C. C.; Donoso, A. *J. Chem. Phys.* **2006***, 125, 154111*.

[47] Hughes, K. H., Wyatt, R. E. *J. Chem. Phys.* **2004***, 120, 4089*.

[48] Shalashilin, D. V.; Child, M. S.; Clary, D. C. *J. Chem. Phys.* **2004**, *120, 5608*.

[49] Heller, E. J. *J. Chem. Phys.* **1991***, 94, 2723*.

[50] Goldfarb, Y.; Degani, I.; Tannor, D. J. *J. Chem. phys.* **2006***, 125, 231103*.

[51] Burghardt, I.; Cederbaum, L. S. *J. Chem. Phys.* **2001***, 115, 10303*.

[52] Husimi, K. *Pro. Phys. Math. Soc. Jpn.* **1940***, 22, 264*.

[53] Dragoman, D. *Physica. Scripta.* **2005***, 72, 290*.

[54] Walkup, R. E. *J. Chem. Phys.* **1991***, 95, 6440*.

[55] Matsumoto, D.; Hayashi, K.; Ida, T.; Mizuno, M.; Endo, K.; Nishikawa, K. *Int. J. Quantum Chem.* **2007***, 107, 3169*.